Polymer 54 (2013) 4404–4421

Contents lists available at SciVerse ScienceDirect

Polymer

journal homepage: www.elsevier.com/locate/polymer

Feature article

Orientation-induced crystallization of isotactic polypropylene

Qi Liu, Xiaoli Sun*, Huihui Li, Shouke Yan*

State Key Laboratory of Chemical Resource Engineering, Beijing University of Chemical Technology, Beijing 100029, China

ARTICLE INFO

Article history:
Received 17 January 2013
Received in revised form
7 April 2013
Accepted 27 April 2013
Available online 17 May 2013

Keywords:
Orientation-induced
Polypropylene
Crystallization

ABSTRACT

In polymer processing operations, the molten polymer chains are frequently subjected to shear or/and elongation flow fields, which will produce molecular chain orientation of the melt. This leads to the orientation-induced crystallization has been an important subject in the field of polymer physics. Systematic studies indicated that the chain orientation influences the crystallization kinetics, the final morphology as well as the polymorphic behavior of the polymers. In this article, the effects of pre-orientation on the crystallization of isotactic polypropylene (iPP) concerning the above mentioned aspects have been reviewed. In particular, the formation mechanism of orientation-induced β-iPP crystallization has been discussed according to the recent experimental results. It is suggested that the local order of the macromolecular chain segments in the melt is most important for β-nucleation of iPP. The formation of β-iPP nuclei may be restricted in a certain chain orientation window of the iPP melts. Chain orientation outside of this window results in the formation of α-iPP.

1. Introduction

Polymeric materials have been widely used in the fields from packaging to aerospace. The reason is that the polymeric materials offer a great potential to meet the requirements for different applications. This rests on the fact that the physical and chemical properties of polymeric materials can be effectively modulated by controlling their structures at different scales. Therefore, it is of great importance to get a fully understanding on the solidification dependant microstructures, which determines the product properties [1–3]. In most polymer processing operations such as injection molding, film blowing, and fiber spinning, the molten polymer chains are subjected to shear or/and elongation flow fields. The shear flow produces chain orientation and affects the crystallization kinetics as well as the crystal structure and morphology of semicrystalline polymers [4–15]. This leads the study of shear-induced polymer crystallization to be an interesting subject for several decades. For this purpose, various devices for imposing shear to the polymer melts have been developed to study the crystallization of polymers under or after shear [10,16–39].

There are a vast body of literature that describe the effects of flow on the crystallization of various polymers as summarized previously in Refs. [39–41]. Among them, isotactic polypropylene (iPP) has been most frequently chosen as model system since (i) its wide applications as conventional plastics; (ii) its lower nucleation density and crystal growth rate at relatively high temperatures, which enable the in situ rheo-X-ray [42–50] and rheo-optical [4,6,8,10,29,45,51–55] studies; and (iii) its diversified structure and morphology, which are sensitive to the changes in processing parameters and molecular parameters such as molecular weight, molecular weight distribution and chain branching etc. [20,46,56]. This makes it ideal to illustrate the influence of shear flow on the solidification behavior of polymeric material in several different aspects.

It is well accepted that external flow causes orientation or even extension of macromolecules in the melt [5,57,58]. Therefore, the flow-induced crystallization of polymers can be referred to as orientation-induced crystallization. Due to the chain orientation, the crystallization behavior of the sheared polymer melt differs notably from its melt crystallization under quiescent condition. First of all, the crystallization rate of a polymer melt with pre-ordered molecular chains can be substantially accelerated [8,9,59–64]. For example, the quiescent melt of isotactic polystyrene crystallizes very slowly. The crystallization of its sheared melt takes place immediately. Moreover, it is well demonstrated that the existence of pre-oriented polymer chains in the melt can influence the crystallization manner and the resultant morphology [9,10,54,65,66]. Generally, oriented structure will form instead of spherulites grown from bulk melt. For polymorphic polymers, shear-flow can also influence the crystal structure. As an example, sheared or strained iPP melt encourages the formation of β-iPP

* Corresponding authors. Tel./fax: +86 10 6445 5928.
E-mail addresses: xiaolisun@mail.buct.edu.cn (X. Sun), skyan@mail.buct.edu.cn (S. Yan).

0032-3861
http://dx.doi.org/10.1016/j.polymer.2013.04.066

crystals rather than its thermodynamically most stable α-iPP crystals, which are always obtained under quiescent condition [10,31,67–69]. The mechanism of iPP β-crystallization in flow field is, however, a long-standing puzzle [70–73]. Taking all these into account, in this article, the effects of chain orientation on the crystallization of iPP concerning the crystallization kinetics, crystalline morphology and crystal structure are reviewed. Particular attention is paid to the formation mechanism of orientation-induced β-iPP crystallization.

The rest of this feature article is organized as follows. In Section 2, a quite brief introduction about the crystallization kinetics of iPP in the flow field is given to show the great progress in this field. Henceforth, the common structural and morphological features of iPP together with their formation conditions are presented in Sections 3 for a better comparison with the orientation-induced structures. The influence of shear flow on the crystalline morphologies of iPP is discussed in Section 4, while Section 5 focuses mainly on the influence of chain orientation on the polymorphic behavior of iPP and the mechanism of iPP β-crystallization. After that the article ends up with a brief summary and future challenges in this subject.

2. Crystallization kinetics of pre-oriented iPP melt

It is well established that polymer chains can be oriented or even stretched by shear flow and consequently crystallize with different kinetics compared to those encountered under quiescent conditions. Therefore, the crystallization kinetics of polymers under shear or elongation flow has been intensively studied [16–18,21–24,28]. We here give a brief introduction to illustrate the great progress in the understanding of the influence of chain orientation on the crystallization kinetics of iPP. For an extensive review please see Ref. [74]. The early studies in this field were focused on the measurements of overall global crystallization kinetics [18,20,25,63,75,76]. The experimental results show that the crystallization process is affected remarkably by the shear flow. An enhancement in the overall crystallization kinetics is seen whenever crystallization takes place during shear or even after shear. Fig. 1 presents an example showing the corresponding Avrami analysis and the increase in the Avrami constant of iPP under isothermal conditions at 136 °C as a function of the shear rate [76]. The change in the Avrami constant k as a function of the imposed shear has been described by $K_{shear} = 2.4\dot{\gamma}^{3.6}$. It indicates that a change of a factor of 2 in the imposed shear rate ($\dot{\gamma}$) could result in a ten-fold increase in the crystallization rate. Undoubtedly, shear rate or shear stress is the most important parameters in shear-induced crystallization of polymers. The shear strain, which is equivalent to the shearing time for a constant shear rate, shows also evident effect on the crystallization kinetics. It was well established that for a constant shear rate, a higher shear strain results in a larger increase in the crystallization kinetics, even though the effect of shear strain (or shear time) is limited at low shear rates.

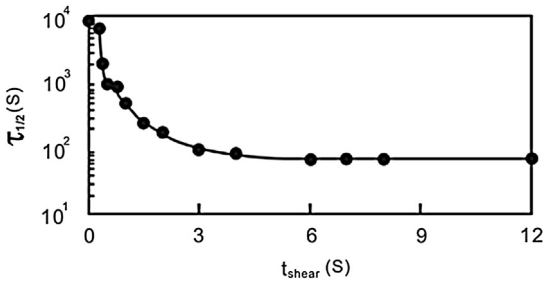

Fig. 2. Turbidity of iPP crystallized following a "pulse" of shear at Tc = 141 °C and $\sigma_w = 0.06$ MPa for various shearing times. The half crystallization time ($\tau_{1/2}$) reaches a plateau after a shearing time of about 5 s. Reproduced with permission from Ref. [8], copyright© 1999, American Chemical Society.

For characterizing the crystallization kinetics of polymers, a quite frequently used parameter is the half crystallization time $\tau_{1/2}$, defined as the time taken to achieve a 50% degree of crystallinity. The influence of flow on the crystallization kinetics of iPP is manifested by a tremendous decrease in the half crystallization time as compared to that for quiescent condition. Due to very fast crystallization of polymers under flow, intensity measurement of transmitted light through a rheo-optical device provided an excellent tool to follow the rapid crystallization kinetics of polymers [51]. In this connection, a turbidity half time ($\tau_{1/2}$), is introduced [8,77]. It is defined as the time where the normalized transmitted light intensity has decayed to its half initial value. Fig. 2 shows a representative result demonstrating the crystallization process of iPP under varying shear conditions. It can be can clearly seen that the $\tau_{1/2}$ for quiescent crystallization was on the order of hours, while it decreases by approximately 2 orders of magnitude upon shearing the melt for 4 s. With the increase of shearing time, the crystallization time first decreases rapidly and then reaches a plateau at a shearing time of about 5 s.

It was suggested that shear flow influences both the nucleation and crystal growth steps. However, the flow-enhanced crystallization rate is predominately attributed to a significant acceleration of the nucleation rate and an increase of nucleus density [30,78]. The common physical intuition is that flow induces local orientation of polymer chains and thus enhances the nucleation ability. In this regard, temperature is very important since it affects the relaxation of the polymer chains or chain segments. For example, a decrease of 20 °C in the crystallization temperature generates a two-order of magnitude acceleration in the crystallization kinetics of iPP. Janeschitz-Kriegl and coworkers have isolated the effects of

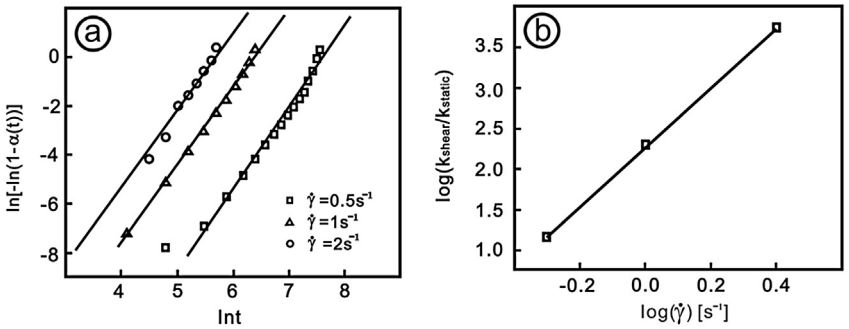

Fig. 1. Avrami analysis: (a) Effect of shear rate at constant shear duration ($t_s = 30$ s) and induction time ($t_0 = 0$ s). (b) Relationship between the kinetic rate constants, k_{shear}/k_{static}, as a function of shear rate for iPP under isothermal conditions at 136 °C. Reproduced with permission from Ref. [76], copyright© 2006, Elsevier Science Ltd.

flow from thermal effects and separated simultaneously the nucleation and crystal growth evens by counting the formed nuclei [29,36,37,79–83]. Their results have demonstrated that the influence of flow on the nucleus density is overwhelming; especially at high temperatures when the number density of nucleus in quiescent melt is extremely small. Moreover, it was found that the number of nuclei increases continuously with increasing duration of the shearing.

It should be pointed out that counting the number of nuclei could only be done at relatively low shear rate and high temperature. At high shear rate, thread like structure forms, which leads to the counting of nucleus number impossible. Therefore, the characterization of the nucleation process of polymer melts under flow is most frequently based on induction time, i.e., the time required for the onset of crystallization, which is suggested to be inversely proportional to the nucleation rate [16,18,20–23,26,28,84]. The determination of induction time is relatively easy through rheology measurement since an abrupt increase in shear viscosity takes place whenever crystallization starts [18,20,21,84]. It was found that the higher the shear rate, the shorter the induction time. Fig. 3 presents a typical dependence of the induction time of sheared iPP melt on shear rate. It shows several features. A most important feature is that they show a zero initial slope, which means the existence of a low shear region where the melt behaves like the quiescent melt. Second, the critical shear rate increases with increasing shear temperature. Another important feature is that the induction time decreases more quickly with increasing shear rate at high temperature. This demonstrates that the effect of flow on the nucleation of iPP is more efficient at high crystallization temperature. The high efficiency of shear on the induced crystallization at high crystallization temperature has been explained in the following way. With increasing temperature the quiescent crystallization rate tends to zero when the temperature closes to its thermodynamic melting point, but the flow-induced orientation effect survives at this temperature. Moreover, Janeschitz-Kriegl and coworkers [79–83] suggested that there is a huge reservoir of poorly organized aggregates (local alignments) of molecular chains. These aggregates can become effective nuclei only at rather low temperatures in a quiescent melt. The flow action can, however, promote the growth of them. In this way, a large amount of poor quality dormant nuclei will be transformed into nuclei with better quality, which are active at a higher temperature under shear.

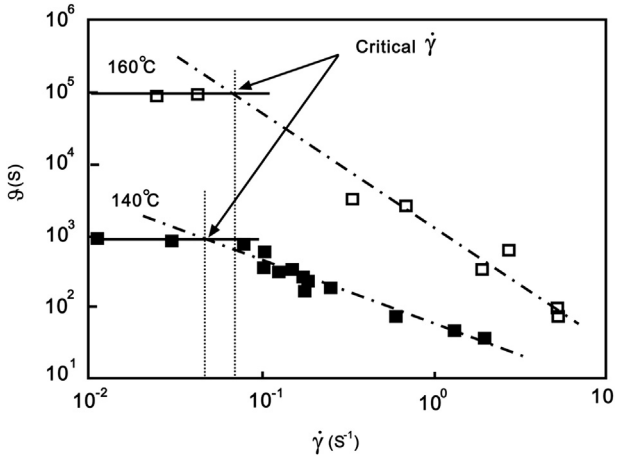

Fig. 3. The induction time of iPP as a function of shear rate. Solid lines indicate the quiescent induction time, while the dashed lines are the linear fits of the high shear rate data. Reproduced with permission from Ref. [139], copyright© 2004, Elsevier Science Ltd.

Therefore, the effect of flow on the crystallization kinetics is relative more pronounced as the degree of supercooling decreases.

The dependence of crystallization rate of sheared iPP melt on the molecular weight and molecular weight distribution supports the above explanations. As reported by several research groups, such as, Janeschitz-Kriegl [37], Winter [51,85], Kornfield [53], and Hsiao [86–88], just to name a few, an increase in M_W results in a larger increase of the flow-induced crystallization rate under the same shear rate. It is widely accepted that for a broad molecular weight distribution sample, only polymer chains above a "critical molecular weight" (M^*) can become sufficiently oriented at a given shear rate [41,46]. In this case, the long molecular chains in a broad molecular weight distributed polymer will be more sheared or stretched with respect to the shorter molecular chains [37,46,51,53]. As a consequence, a small amount of high molecular weight tail leads to an absolutely faster crystallization of a sheared iPP melt.

The above discussion has qualitatively explained the observed phenomena of the flow effect on the iPP crystallization. Actually, phenomenological models based on the fundamental work of quiescent isothermal crystallization kinetics have also been proposed to describe the flow-induced polymer crystallization [5,75,89–96]. McHugh has made the first attempt for extending the theory for quiescent condition to flow-induced crystallization [90]. In their case, the same expression for quiescent nucleation rate was chosen with the addition of a driving force term [97]. Grizzuti and coworkers [75,95,96] have considered the coupling between temperature and flow under isothermal conditions and modified the flow-induced crystallization model for describing the early stage of isothermal crystallization of sheared polymer melts. Further improvement of their model has been made by the calculation of free energy change of a polymer chain during flow in terms of the Doi–Edwards micro-rheological theory [98]. Based on the assumptions that (i) the flow mainly affects the nucleation process [29], and (ii) the effect of flow on the nucleation rate is merely additive and leads to an increase in the thermodynamic driving force for nucleation, they have modified the free energy difference between liquid and crystalline phase. It should be emphasized that the proposed theoretical model is successful not only for a qualitatively explanation of the observed experimental phenomena, but also for a quantitative prediction of the induction time of iPP under steady shear flow at isothermal conditions since the related parameters can be obtained from independent experiments [75,96].

3. Basic structure and morphology of iPP

The last paragraph has briefly summarized the great progress in the study of crystallization kinetics of pre-oriented iPP melt. Henceforth, the influence of shear flow on the crystalline morphology and crystal modification of iPP will be discussed. To this end, the common structural and morphological features of iPP together with their formation conditions are presented first for a better comparison with the orientation-induced structures. IPP is a semicrystalline polymer with pronounced structures and morphologies depending on the processing and molecular parameters [20,46,56]. It is clear that the iPP chains possess always a 3/1 helical chain conformation in the crystal. However, the existence of left- or right-handed helical chains made the crystalline architecture and morphology of iPP multifaceted. Depending on the tacticity, molecular weight, thermal treatments and mechanical handling, the iPP can pack in three different crystalline structures, designated as α, β and γ forms [99–107]. Moreover, a so-called smectic mesophase, which is sometimes referred to as a conformational disordered phase, has also been reported [108,109].

Table 1
Types of iPP spherulites.

Spherulite type	Banding	Birefringence (Δn)	Crystallization temperature
α_I	No	0.003 ± 0.001	<134 °C
α_{II}	No	-0.002 ± 0.0005	>138 °C
α_m	No		134–138 °C
β_{III}	No	−0.013	<128 °C
β_{IV}	Yes	−0.023 (bright) & −0.002 (dark)	128–132 °C

The α-iPP, which can be simply produced by melt crystallization of commercial grade iPP under static condition, exists in a monoclinic lattice with alternate layers of left- or right-handed helices along its *b*-axis direction [2,100]. Different types of α-iPP spherulites depending on growth condition have further been classified by Padden and Keith on the basis of their optical birefringence [101,110]. As listed in Table 1, spherulites grown below 134 °C have a slightly positive birefringence (the type referred to as α_I), whereas spherulites grown above 138 °C have a negative birefringence (the type referred to as α_{II}). When the crystallization temperature is set between 134 and 138 °C, spherulites often display a mixed birefringence and are therefore referred to as 'mixed' type (α_m). The temperature-dependent optical behavior of α-iPP spherulites is quite complex. There exist discrepancies in the temperature ranges for α-iPP spherulites grown by different researchers. This may be associated to the used materials. Moreover, the optical characters of α-iPP spherulites could change by thermal treatment. It was found that high temperature annealing can lead to a transformation from positive or mixed α-iPP spherulites into negative ones. The structural origin of the peculiar birefringence feature was explained using the unique wide angle lamellar branching of α-iPP [73,102–104]. The wide angle lamellar branching creates a cross-hatched bimodal lamellar orientation with the radial lamellae initiating the overgrowth of the nearly tangential oriented lamellae. It is an intrinsic property of α-iPP and happens under many crystallization conditions, e.g., growth from thin molten layer (see Fig. 4a) [111] and in solution cast thin films (see Fig. 4b) [112]. Even though the phenomenon was first observed in the early 1960s, an understanding of it on a molecular level was achieved nearly 20 years later [73,102,104,105]. Taking the molecular subgroups, i.e., the side methyl groups, and the handedness of the helices into account, Lotz et al. [73] has explained that the branching takes place whenever two successive *ac* layers are made of chains with the same hand (see Fig. 5), whereas the crystallographic unit cell requires opposite handed helices.

According to the "cross-hatching" model, the peculiar positive and mixed birefringence was associated to the existence of tangential oriented lamellae in the spherulites. For a better understanding, Fig. 6 shows a polarized optical micrograph, using a primary red filter (λ-plate), of α-iPP spherulites. The inner and outer parts of each spherulite are optically positive and negative, respectively [113]. Scanning electron microscopy observations illustrate the fine lamellar structures of both inner and outer parts of the α-iPP spherulites. As presented in Fig. 7, it is obvious that the growth character of the central part of the spherulite is different from the outer part. In the outer part, most of the lamellae grow along the radial direction of the spherulites, reflecting the conventional spherulite growth character of most polymer spherulites. On the other hand, the inner part of the spherulite exhibits an interwoven structure with the lamellae oriented preferentially both in the radial and tangential directions. The adjacent lamellae lay approximately orthogonal (ca. 80°) to each other, forming a cross-hatched structure. This provides the direct evidence that the negative α-iPP spherulites are characterized by predominantly radial lamellae while the positive spherulites are characterized by a cross-hatched lamellar morphology. Based on the above description, one can easily imagine that the 'mixed' spherulites are the consequence of inhomogeneity in a given spherulite with the coexistence of radial and tangential predominant domains.

The β-iPP is thermodynamically metastable. Even though it was first observed in 1959 [109], its crystal structure has been a puzzle for a long time and was just solved in 1994 [71,72]. The reason for the delay rests on the uncertainty of the unit cell dimensions and symmetry. Difficulty in solving the β-iPP crystal structure stems from the fact that its fiber pattern cannot be obtained since βα conversion takes place during stretching. This leads to the suggestion of various hexagonal unit-cells with the *a*-axis parameter ranging from 1.1 to 2.2 nm [106,114–116]. A sophisticated understanding of β-iPP structure has been realized by detailed electron diffraction analysis of its single crystals. It is now clear that, in the β phase, the iPP molecular chains of three-fold isochiral helices build up trigonal unit cell with different azimuthal orientations. The helices thus have different environments and at least one of these environments is less favorable, i.e., the formation of frustrated packing of helices [21,72]. The spherulites of β-iPP exhibit very strong negative birefringence in comparison with its α-counterparts and have been divided into two categories as also listed in Table 1, i.e., the radial β_{III} and ring banded β_{IV}. It was confirmed that the banded β-spherulites contain lamellae twisted around their longitudinal axes. In the dark bands, lamellae lying flat-on are dominating, while the bright bands represent the regions where the lamellae stand on their edges [22,23,117,118]. Moreover, hedritic structures of β-iPP could form at high crystallization temperature, which exhibit regular polygonal forms [24–26,119–121]. The appearance of the hedrites depends remarkably on the direction of view and the maturity of the structure. Several forms have been recognized. They are mainly: (i) hexagonites in hexagonal shape with weak birefringence, (ii) axialites with strong negative

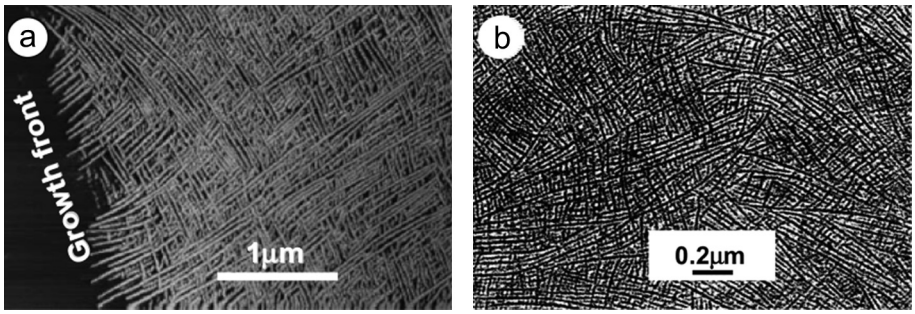

Fig. 4. Cross-hatched lamellar structures of iPP formed under different conditions. (a) An AFM phase image taken during isothermal crystallization of iPP from melt at 146 °C. (b) A phase contrast TEM micrograph taken from a solution cast iPP thin film at 110 °C. Part a is reproduced with permission from Ref. [111], copyright© 2005 Elsevier Science Ltd.

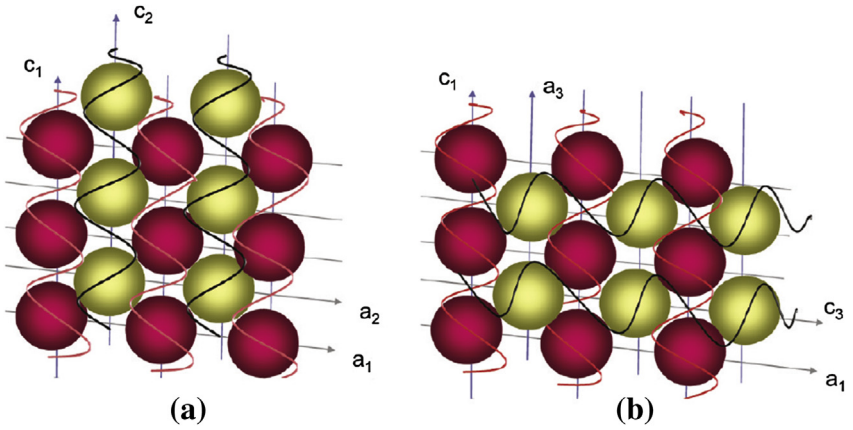

Fig. 5. A schematic representation of the wide angle lamellar branching of α-iPP and the interactions between facing methyl groups of parallel *ac* planes made of either isochiral or antichiral helices. (a) Illustration of parallel deposition of the i-PP helices on the *ac*-plane of the α-phase giving rise to a continuous α-phase growth. The methyl groups of the substrate growth face (a_1c_1-plane) are shown as red balls. The yellow methyl groups of the depositing antichiral stems in the a_2c_2-plane face and are interdigitated with the red methyl groups which are the stem orientation in the new layer is parallel to in the original α-phase crystal (a_1 is parallel to a_2, and c_1 is parallel to c_2). (b) Molecular deposition of the i-PP helices on the *ac*-plane of the α-phase leading to the lamellar branching in i-PP. The yellow methyl groups are now of helices isochiral to the substrate ones. A pattern of interactions similar to (a) is generated when the stem orientation in the a_3c_3-plane is either 80° or 100° away from that in the original α-phase crystal (a_3 is parallel to c_1, and c_3 is parallel to a_1). Adapted from Ref. [73].

birefringence, (iii) ovalites in oval form developed from the axialites in later stage of crystallization, and (iv) quasi-spherulites developed either from hexagonites or axialites. These hedrites are regarded as the precursors of β-spherulites since transformation of them into spherulites generally takes place in the later stage of growth [24,120].

The γ phase of iPP has received much less attention. This leads to the early work being not well continued for a long time [31,32,122,123]. The breakthrough in the understanding of γ-iPP crystal structure has been realized in the 1990s after Meille and Bruckner reported a non-parallel chain packing in an orthorhombic unit cell [124]. The non-parallelism of iPP chains in the γ-phase has actually a close resemblance with the lamellar branching of α-iPP in a way that the chain axis rotation of lamellar branching in α-iPP has become a crystallographic element of symmetry in the γ-iPP unit-cell. Actually, the γ-iPP crystals usually co-crystallize with their α counterparts under special conditions, such as, low M_w specimen, crystallization of conventional iPP under high pressure or incorporation of a few percent of comonomer at atmospheric pressure [125–131]. The achievement in producing well-defined iPP copolymers with high stereoregularity and large content of comonomers has revived the studies on chemical and physical requirements for the formation of γ-iPP [130–132]. Morphological analyses show that the γ-iPP spherulites can be optically positive or negative depending upon the crystallization temperature [17,19,56,109].

The smectic phase or conformational disordered phase of iPP reflects a well-defined phase with an extent of order intermediate between the crystalline and amorphous phases [2,100,107,108]. It has also been less frequently named as paracrystal [35,133], microcrystal [36], condis crystal [37,134], or mesomorphic phase [38,135]. In this phase, the chains have undergone a conformational ordering from random coil to 3/1 helix, but the packing of helices are not as that in the crystalline phase. It is often characterized by parallel helices with some degree of positional correlation along the chain axis between adjacent helices but disorder in the lateral

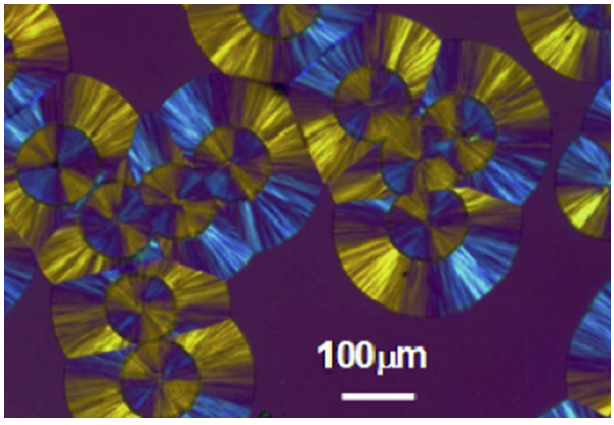

Fig. 6. A polarized optical micrograph, using a primary red filter (λ-plate), of α-iPP spherulites. The sample was prepared by crystallizing the iPP from melt at 138 °C for 30 min, then heated again to ca. 174 °C, at which the birefringence disappears completely, and finally cooled with a cooling rate of 30 °C/min to 138 °C for 40 min isothermal recrystallization. The inner parts of the spherulites correspond to the parts first crystallized at 138 °C, melt at 174 °C and then recrystallized at 138 °C again, while the outer parts are those grown directly from the melt at 138 °C after cooling from 174 °C to 138 °C. Reproduced with permission from Ref. [113], copyright© 2006, Wiley-VCH.

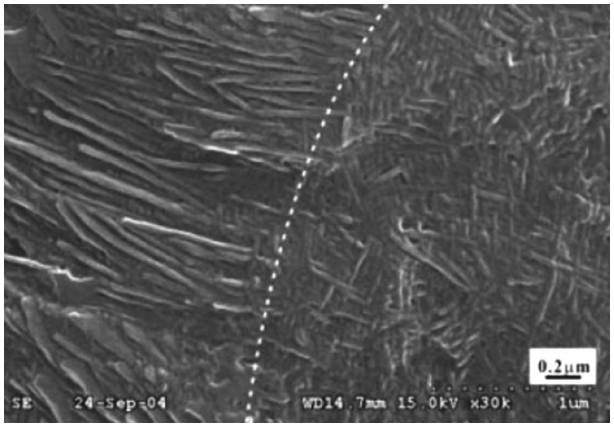

Fig. 7. An SEM micrograph shows a boundary area including the fine structures of both inner and outer parts of the α-iPP spherulites presented Fig. 2. The right side corresponds to the inner part, while the left side corresponds to the outer part. Reproduced with permission from Ref. [113], copyright© 2006, Wiley-VCH.

packing. In general, this phase can be produced by cold-drawing and quenching the melt at a drastic cooling rate, which is considered as a "frozen" intermediate ordering state during crystallization pathway [37,134].

4. Orientation-induced morphology of iPP

When polymers crystallize from melt subjected to flow, the semicrystalline morphology changes due to the existence of chain orientation [136]. This is reflected by the change from typical spherulite shape encountered under quiescent condition to the highly oriented structure. Fig. 8 presents a transmission electron micrograph and its corresponding electron diffraction pattern of the uniaxially oriented iPP thin films crystallized under elongation flow. It was prepared according to the melt-draw technique introduced by Petermann and Gohil [137]. In the bright field image, one can see the highly oriented crystalline lamellae parallel aligned perpendicular to the flow direction. The sharp and well defined electron diffraction spots demonstrate the excellent chain orientation of the iPP. All of the observed electron diffraction spots can be accounted for by a monoclinic unit cell with lattice constants $a = 0.666$, $b = 2.078$, $c = 0.650$ nm and $\beta = 99.62^\circ$ [100], indicating the formation of oriented α-iPP crystals.

Another most frequently encountered morphology formed under flow condition is the "shish–kebab" structure [3,41–44,46,49,75,138–161]. It is generally accepted that molecular chains of a polymer could be stretched under flow field. The stretched molecular chains form extended chain "shish" crystals, which initiate the overgrowth of folded chain "kebab" crystals. The first theory dealing with chain dynamics of polymers in dilute solution under flow has been developed by de Gennes [162]. The core of his theory was the abrupt coil–stretch transition; i.e. polymer chains undergo a sharp transition from random coil to a fully extended-chain conformation. Keller et al. [138] have provided the experimental evidence for the coil–stretch transition of polymer crystallization in dilute solutions under flow and proposed a molecular model of the "shish–kebab" structure. Taking this into account, the "shish–kebab" morphology can be used as a signature of the occurrence coil–stretch transition. Similar to those observed in dilute solutions, the coil–stretch transition was also found in entangled iPP melts, which leads to the formation of "shish–kebab" structure of iPP under shear flow.

To understand the origin of "shish–kebab" structure of iPP, Han et al. [155–158] have investigated the shear-induced crystallization of iPP at low shear rate (shear rate $< 1\ s^{-1}$) and low temperature. They have observed the shear-induced cylindrite structures. As shown in Fig. 9, the core of the cylindrites formed rapidly after shear cessation. The length of the core did not change after shear cessation. However, it initiates the growth of the crystals laterally. At late stage quantity of the newly formed crystals impinged into each other. From the AFM images of the etched iPP samples, the shish-like structure was found to be much wider. Compared with the radius of gyration of the used sample, it is suggested that the process of shear-induced shish crystals may involve a large number of entangled molecules under a low shear rate and low temperature. According to these results, a schematic illustration of the shish–kebab structure under shear at low shear rate is presented in Fig. 10.

Shear induced shish–kebab morphology has also been achieved and monitored by AFM, as presented in Fig. 11. The shear force was introduced by controlling the value of setpoint and moving the cantilever a certain distance under the lift mode. Based on the results, several points have been identified. First of all, the morphology of shish–kebab depends on the shear stress. Under low shear stress, the distance of two adjacent kebabs is large ($\approx$16 nm) and the thickness of the kebabs is much thinner than that of shish structure. With increasing shear stress, the kebabs pack much more densely. Second, the relaxation time at shear temperature determines the length of shish crystals. With the increase of relaxation time, the overall length of the shish structure shortens through fracturing into several parts. When the relaxation time is longer than 480 s, only very short shish structure can be observed. At the same time, the ability of the shish for inducing the kebab lamellae weakens. Third, the in situ melting experiment suggests that the unoriented lamellae melt first at the nominal melting temperature (about 167 °C), followed by the melting of kebab lamellae at a relatively higher temperature (174 °C), and finally the shish structures melt at an even higher temperature (180 °C). This indicates that the shear induces the formation of shish–kebab crystals of iPP in its α-phase.

Hsiao et al. [43–46,144–150,163] have studied the formation of shish–kebab structure of entangled iPP melt by in situ rheo-X-ray and revealed the early stage of the shear-induced crystallization. Through combined SAXS and WAXD experiments, they found that scaffold (network) of precursor structures forms at the early stage, which may correspond to the density fluctuation prior to crystallization. This was also found by the in situ rheo-optical investigation of the flow- or shear-induced crystallization of iPP under oscillatory shear [51,164–166]. The scaffold containing shish crystals with extended chain conformation can exist in amorphous [45], mesomorphic [148] or crystalline [164] states while the kebabs with fold chain conformation exist only in the crystalline state. The chains in the shish crystals were entangled with the neighboring chains. The individual chains do not disentangle completely in the deformed melt and undergo abrupt unwinding to fully extended chain conformation. It was further found that the core of the cylindrites comes from stretched bundles of the entangled network strands rather than from the extended chains in stretched melt.

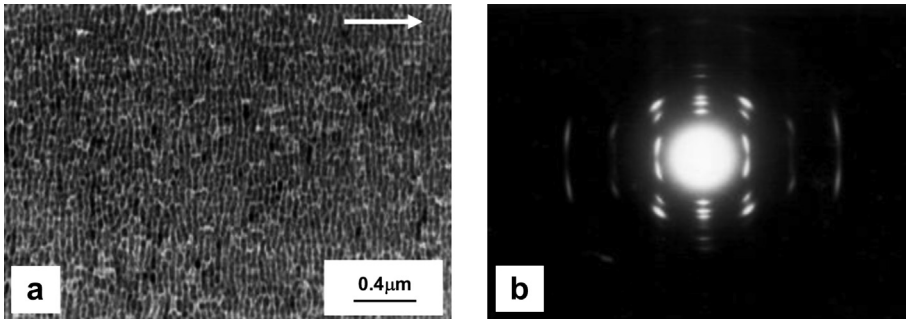

Fig. 8. (a) A bright field transmission electron micrograph and (b) its corresponding electron diffraction pattern of the highly oriented iPP thin films crystallized under elongation flow through melt-draw at 130 °C. The arrow indicates the drawing direction.

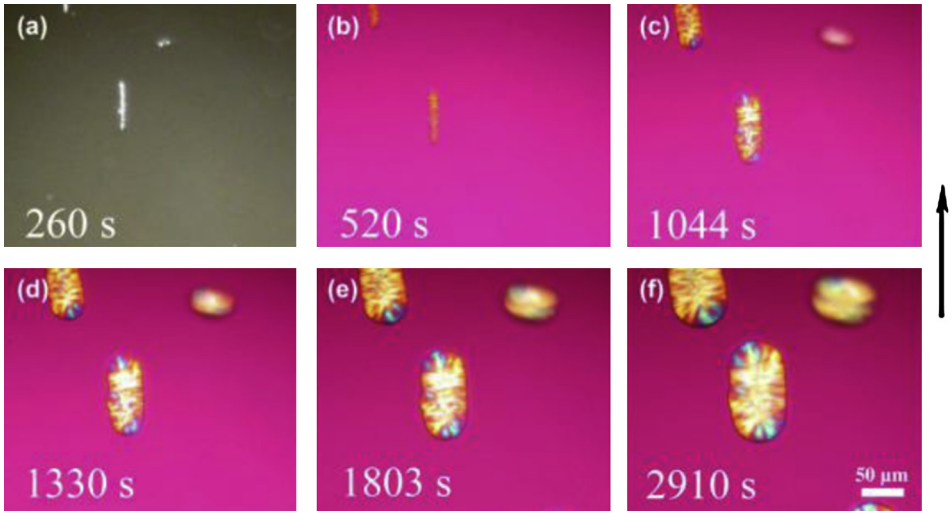

Fig. 9. Optical micrographs of the shish-kebab-like structure grown from sheared iPP melt. The thermal history of the iPP was melted at 200 °C for 5 min, then quenched to 140 °C and sheared for 2 s at shear rate of 0.5 s^{-1}. After shear cessation, the sample was isothermally crystallized at 140 °C for different times. The arrow indicates the flow direction. Reproduced with permission from Ref. [156], copyright© 2007, Elsevier Science Ltd.

Moreover, the average length of shish-like structure decreases instead of increasing with time after shear.

5. Orientation-induced polymorphic behavior of iPP

As mentioned in the third section, iPP is one of the polymers exhibiting pronounced polymorphism depending upon the thermal and mechanical treatments. The α modification can be easily produced by melt crystallization of commercial grade iPP under static condition [100]. The β form is difficult to be obtained under normal processing conditions and therefore has been considered as laboratory curiosities. Nevertheless, it attracts due attention owing to its different performance characteristics, including low crystal density, low melting temperature, and markedly improved impact strength and toughness [167–188]. It was found that crystallization from sheared or strained iPP melt encourages the crystallization of iPP in its β-phase [9–11,42–44,65–70,170,189]. Studies in this field concern mostly the effect of shear rate on the β-crystallization of iPP. The mechanism of its β-crystallization remains a long-standing problem.

Steady shear experiments with rotational plates show that the β-iPP crystals can be created at very low shear rate. Fig. 12 presents the optical micrographs of an iPP sample prepared by shearing the iPP supercooled melt at 134 °C for 5 s at a shear rate of only 1 s^{-1} [156]. Selective melting at 156 °C demonstrates the existence of the β-iPP crystals. It was found that the amount of β-iPP crystals depends evidently on the shear rate. Hsiao et al. [44,190] found that

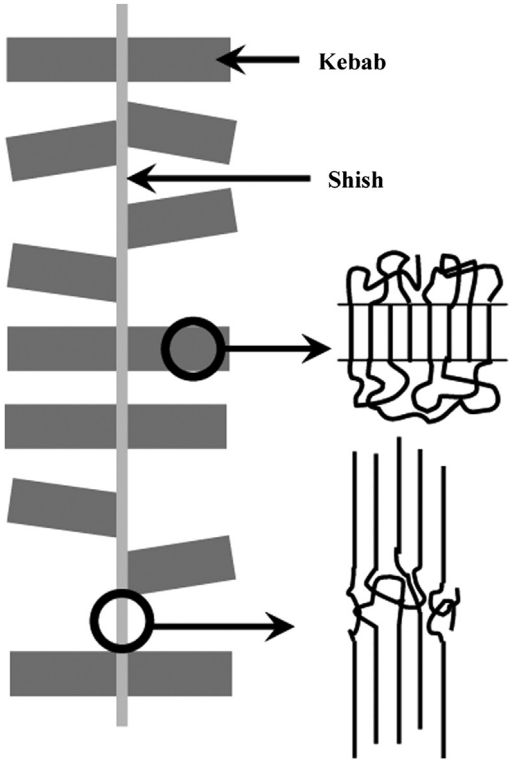

Fig. 10. Illustration of shish–kebab structure formed under shear at low shear rate.

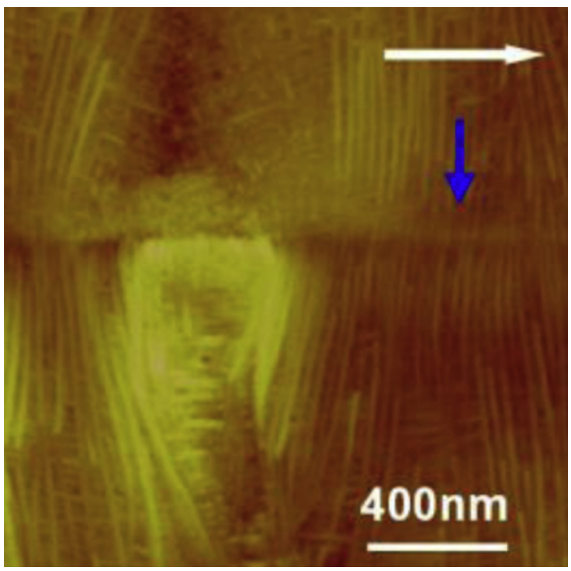

Fig. 11. An AFM image shows the shear induced shish–kebab morphology (indicated by an blue arrow) achieved under AFM. The sample has been sheared by the AFM tip and relaxed for 120 s after shear. The white arrow indicates the shear direction.

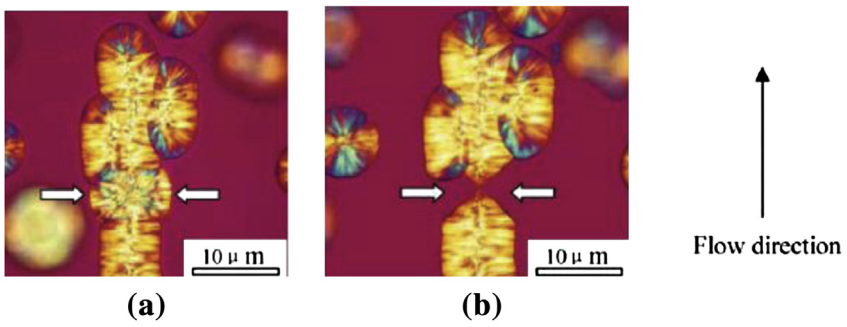

Fig. 12. (a) An optical micrograph of iPP crystallized under shear. The sample was prepared by melting at 200 °C for 5 min, then quenched to 134 °C and sheared 5 s at the shear rate = 1 s^{-1}, followed by isothermal crystallization at 134 °C for 500 s. (b) The selective melting of the β-form iPP at 156 °C (indicated by the arrows), indicating the formation β-iPP under used shear condition. Reproduced with permission from Ref. [155], copyright© 2005, Elsevier Science Ltd.

the amount of β-phase reached a plateau value at a shear rate of 57 s^{-1}, while a 70% final contribution of β-iPP crystals to the total crystalline phase was reported at the shear rate of 102 s^{-1}. An et al. [191] have studied the development of both α and β iPP crystals in the iPP melt after shear as a function of shear rate. They found that the total crystallinity of iPP is not affected by the shear rate, while the portion of the β crystals depends remarkably on the shear rate. With increasing shear rate, the contribution of β-iPP crystals to the total crystalline phase increases rapidly and reaches a maximum at a shear rate of ca. 20 s^{-1}. Henceforth it decreases slightly with further increase of the shear rate. This is somewhat different from the result reported by Hsiao et al. The inconformity may be caused by different materials used. On the other hand, WAXD experiments demonstrated that the intensity of the $(300)_\beta$ reflection did not show noticeable azimuthal dependence. This means that the β-crystals were primarily unoriented. From this point, the increase in the crystallization kinetics of unoriented crystals concluded from the SAXS study may be attributed to the β-crystallization of the iPP. Moreover, the oriented α-crystals form immediately after shear and then the β-crystals grow subsequently suggests that the surface of the oriented α-crystal entities may provide nucleation sites for the β-crystals. These results just provide us some speculations about the formation mechanism of β-iPP crystals. Detailed information about shear-induced β crystallization of iPP has been obtained by fiber pulling procedure, in which the shear-induced crystallization of iPP was performed by pulling the fiber embedded in iPP melt along the fiber axis [33,66,192].

It was attested that the fiber-pulling process was efficient in producing samples rich in β-modification, regardless of the nucleation abilities of the used fibers toward the iPP matrix. For example, the unsized glass fiber shows no nucleation capability towards iPP in static melt but induces column structures of iPP by pulling the fiber during crystallization of iPP matrix [30,65]. Even for the fibers which can nucleate the iPP, the supermolecular structures of iPP induced by shear created through fiber pulling are different from those in the transcrystalline zone formed in static melt. When crystallizing from static melt, the monoclinic α-iPP was the observed morphology in the vicinity of the fibers as well as in the areas of bulk crystallization. In the shear-induced crystallization of iPP through fiber pulling, mainly β-iPP crystals were produced in the vicinity of the fibers. To distinguish the column structure generated by fiber pulling from the transcrystalline structure triggered by surface induced heterogeneous nucleation, Varga et al. [66] have defined the shear-induced column structure as "cylindrite". Through selective melting of the β-iPP crystals at temperatures above the melting point of β-iPP but below that of α-iPP (e.g. 160 °C), they found that the shear-induced supermolecular structure consisted of two crystalline forms, namely, a thin α-iPP layer directly connected to the pulled fiber with a zigzag outline and the later grown β-iPP layer away from the fiber. Based on this fact, it was concluded that shearing the iPP melt by fiber pulling yielded primary α-row nuclei along the fiber. As sketched in Fig. 13, on the surface of these α-row nuclei, a α-to-β growth transition or αβ-bifurcation took place during crystal growth, which led to the formation of randomly dispersed point like β nuclei. These β nuclei induce a layer with β-phase in rich along the pulled fiber as long as a higher growth rate of the β-phase (G_β) than α-phase (G_α) was achieved [10,70,193,194]. Otherwise, the quickly growing α-iPP crystals would embed the generated β-nuclei. A faster growth rate of β-iPP crystals than its α-counterparts can only be achieved in the temperature range of 100–140 °C. Therefore, the αβ-growth transition is also limited in this temperature window. The fact that the oriented α-crystals always form first and then the β-crystals grow afterward seems to support the present explanation since the existence of α row nuclei in shear-induced crystallization has been proved by optical microscopy and AFM observations [10,66,70,121]. Also the β crystallization of iPP in a temperature gradient can be well explained in terms of αβ-growth transformation along the oriented α growth front [171,172]. There are, however, two aspects which remain difficult to be understood, namely, (i) the occurrence

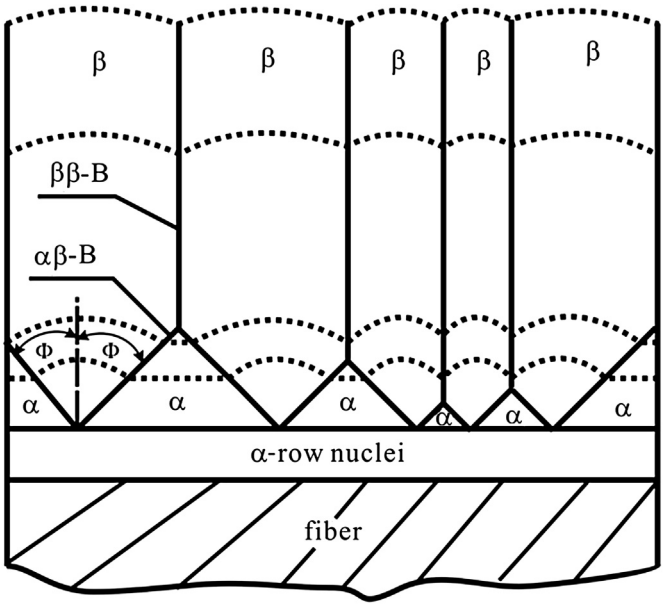

Fig. 13. Schematic diagram of a cylindrite structure with αβ bifurcation. Reproduced with permission from Ref. [202], copyright© 2006, American Chemical Society.

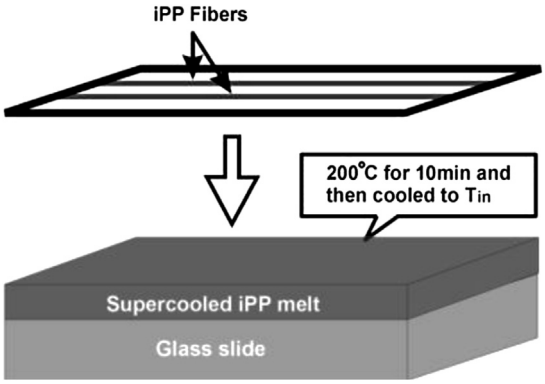

Fig. 14. A sketch shows the sample preparation procedure of single iPP fiber/matrix composites. Reproduced with permission from Ref. [195], copyright© 2003, American Chemical Society.

of the αβ-growth transition on the surface of the in situ formed α-row nuclei instead of the growth of α-iPP crystals and (ii) the original morphological difference on the α-row nuclei surface between the places where the αβ-growth transition taking place and the continuous growth of α-iPP crystals, i.e. the bottom edges of the α-iPP triangles shown in Fig. 13. In other words, the origin behind the αβ-growth transition, if it exists, is still not quite clear.

To disclose the origin of shear-induced β-crystallization of iPP, our group has adopted another way to follow the orientation-induced crystallization of iPP [195–203]. In our procedure, we check the orientation-induced crystallization of iPP by recrystallizing its highly oriented fibers after incomplete melting of them. Here the orientation of the iPP molecular chains is controlled by the melting temperature and relaxation time of the fibers. Considering that the morphological features of the single fiber are difficult to be monitored, self-induced crystallization of iPP melt by its homogeneous fiber with varying melting extent was studied. The fiber/matrix single iPP composites were produced by a procedure sketched in Fig. 14. The iPP matrix thin film was first heated to 200 °C for 10 min to erase possible effects of thermal history on the subsequent crystallization of the sample and then moved to a preheated hot plate, where the iPP matrix was kept in the molten or supercooled molten state at the moment of fiber introduction. As the iPP molten or supercooled molten thin layer reached equilibrium at the desired temperature, homogeneous iPP fibers tightly fixed on a metal frame (see upper part of Fig. 14) were introduced into the iPP matrix. After introduction of the fibers, the prepared fiber/matrix single iPP composites were subsequently moved quickly to another hot plate set at desired temperature for isothermal crystallization. In the henceforth paragraphs, we review our recent results and discuss their implications for the orientation-induced β-iPP crystallization mechanism.

We first check the importance of crystallization rate for the β crystallization of iPP. During our experimental procedure, we do find that by melting the iPP fiber at temperatures slightly over its nominal melting point for short time, mainly β-iPP cylindrical structures are observed after crystallization in the temperature window of 100–138 °C (see Fig. 15a, b and c), while α-iPP cylindrical structures are generated at crystallization temperatures above 140 °C (see Fig. 15d) [197]. This is, however, not necessary to indicate that a higher G_β is sufficient for the β crystallization of iPP. The interfacial morphology created by crystallization at 139 °C under otherwise unchanged parameters is particularly helpful for elucidating the effect of crystal growth rate on the β-iPP crystallization. As presented in Fig. 16, now both α-iPP and fan shaped β-iPP crystals are observed in the transcrystalline layers of iPP. Comparing the growth fronts of the α- and β-iPP crystals, one can find that the β-iPP crystals possess an evident higher growth rate than its α-counterpart. The formation of β-iPP transcrystalline structure is, however, suppressed. This clearly implies that a higher G_β may be necessary but not sufficient for promoting β-iPP crystallization. The nucleation of β-iPP crystals is the prerequisite for β-iPP crystallization.

According to the above experimental results, we focus our attention on the nucleation of β-iPP crystals by adjusting the fiber introduction temperature. For this purpose, the crystallization temperatures in all experiments were set in the temperature range

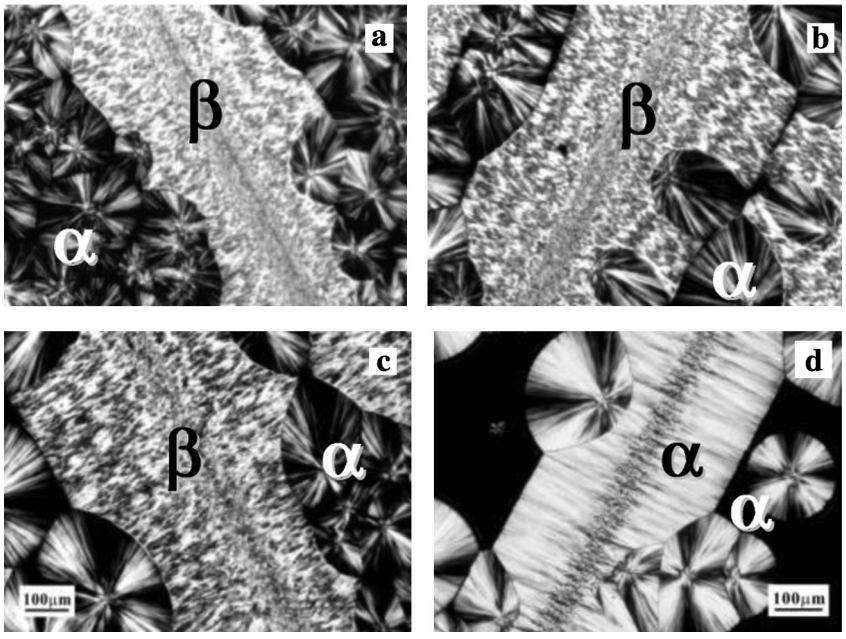

Fig. 15. Optical micrographs of iPP single-polymer composites with α and β iPP crystals indicated. The fiber introduction temperature was 173 °C and the isothermal crystallization temperatures were (a) 126 °C, (b) 130 °C, (c) 133 °C and (d) 141 °C. Reproduced with permission from Ref. [197], copyright© 2004, Elsevier Science Ltd.

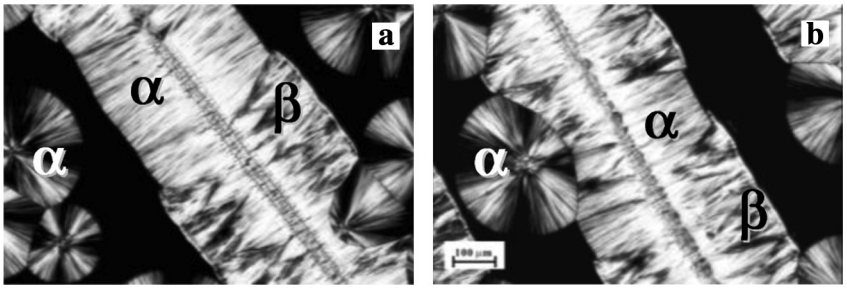

Fig. 16. Optical micrographs of an iPP single-polymer composite with α and β iPP crystals indicated. The fiber introduction temperature was 173 °C and the isothermal crystallization temperature was 139 °C. Reproduced with permission from Ref. [197], copyright© 2004, Elsevier Science Ltd.

for a higher G_β. Optical microscopy observations show that if the iPP fibers were introduced into the supercooled iPP matrix at temperatures far below the melting point of iPP fiber ($T_m \approx 170$ °C), e.g., below 160 °C, the iPP fiber is kept in the solid state without any melting. In this case, it illustrates simply the crystallization of iPP matrix induced by its homogeneous fiber. As shown in Fig. 17, the morphological difference between iPP in the vicinity of its homogeneous fibers and in the areas away from the fibers unambiguously indicates that the iPP matrix was indeed kept in supercooled molten state at the moment of fiber introduction. Two different morphologies of the sample were produced. One is the column structure of iPP matrix surrounding its single polymer fibers, while the other one is the spherulitic structure of iPP matrix away from the fibers. Melting test demonstrates that both spherulitic and column structures are composed of monoclinic α-iPP. This has a close resemblance with what obtained by Loos et al. [204] The same negative optical character of the interface layers surrounding the iPP fibers as well as the matrix spherulites indicates a similar lamellar arrangement in both regions. Moreover, the density of the iPP nuclei generated on its own fiber surface is too high to resolve each individual one on an optical level, even in the enlarged optical micrograph, Fig. 17b.

Scanning electron microscopy (SEM) helps to disclose the fine interfacial structure. As shown in Fig. 18, the smooth surface and well-defined boundary of the iPP fiber, which is located near the left side edge of the picture, indicates that the iPP fiber is not molten. From the fiber surface, one sees parallel-aligned α-iPP crystalline lamellae grown transversely, indicating the high nucleation ability of the iPP fiber toward its single polymer matrix. The discontinuity of the crystalline lamellae allows the crystallization to occur in other inaccessible regions. The characteristic lamellar branching of α-iPP appears between the parallel aligned lamellae [205,206]. Unlike crystallization from the bulk, the daughter lamellae are thinner than the mother ones and further branching on the daughter lamellae has been suppressed. It implies that the rejected materials produce the daughter lamellae during the cooling process of the sample. The optical character of the iPP spherulites depends on the relative proportion of the two populations of radial lamellae and tangential lamellae and it relies also on the orientation of the radial lamellae relative to the path of light [113,206]. The fine structure disclosed by SEM supports the conclusion made by optical microscopy observation.

With increasing fiber introduction temperature, fan-shaped β-iPP domains sporadically inlaid in the α-iPP column layers have been occasionally observed. When the fibers were put into the matrix at temperatures close to its nominal melting point, e.g., 168 °C, substantive β-iPP crystals can be created. Fig. 19 shows the representative optical micrographs with β-iPP crystals distributed unevenly along the fibers. Around the top part of the left fiber (see Fig. 19a), the iPP grows mainly in its crystalline β phase, whereas the fiber on the right side of the picture is predominantly surrounded by the α-iPP crystals. In the middle of the picture, different supermolecular structures of iPP matrix are generated on different sides of the same iPP fiber, i.e. the α-iPP and β-iPP on the right and left sides of the same iPP fiber, respectively. The different crystallization manners may be associated with either the different local thermal condition of the sample or the different local nature of the fiber. Anyway, this is quite helpful for exploring the different growth mechanisms of the α-iPP and β-iPP crystals. With careful comparison, one can find the different responses of the iPP fibers in different areas during thermal treatment. The fibers in the areas where β-iPP crystals are generated seem to be molten, see upper left corner of Fig. 19a. The fiber located at the middle of the picture becomes thinner and thinner from its bottom to top ends, suggesting a partial melting of the iPP fibers. This phenomenon is more clearly seen from the magnified optical micrograph as illustrated in Fig. 19b. At the right side of the bottom end of the iPP fiber, the existence of well defined boundary line between the iPP fiber and the induced crystalline α-iPP (as indicated by an "α") indicates that the iPP fiber remains intact during the thermal treatment. On the

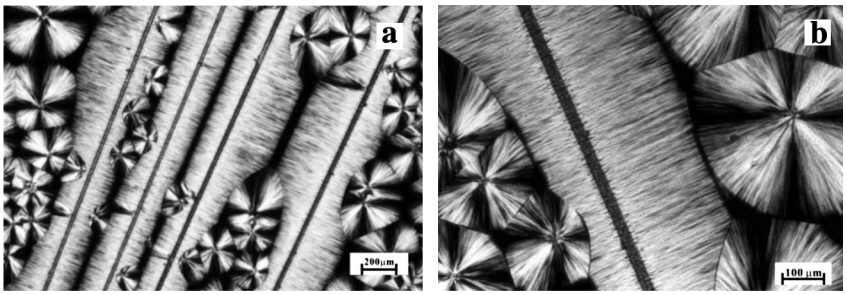

Fig. 17. Optical micrographs of an iPP single-polymer composite, which show only α-iPP crystals. The fiber introduction and the isothermal crystallization temperatures were 138 °C. Reproduced with permission from Ref. [195], copyright© 2003, American Chemical Society.

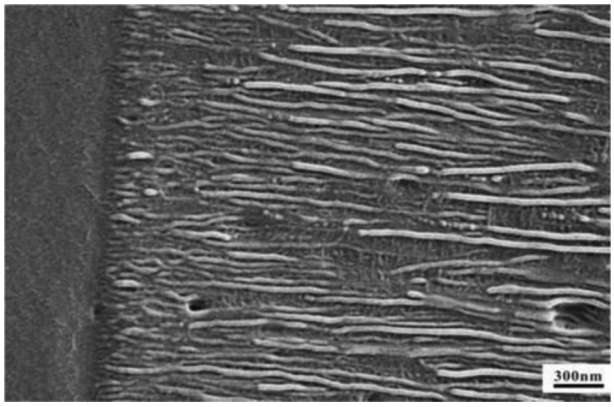

Fig. 18. A SEM micrograph shows the α-iPP edge-on lamellae grown from the surface of the α-iPP fiber. The introduction temperature of iPP fiber, located at the left side edge of the picture, was 158 °C. The sample was isothermally crystallized at 135 °C for 1 h after the fiber introduction. Reproduced with permission from Ref. [199], copyright© 2004, American Chemical Society.

contrary, the top part of the iPP fiber surrounded by β-iPP crystals can hardly be distinguished from the iPP matrix, indicating the inosculation of the iPP fiber with its homogeneous molten matrix through melting or at least surface melting. This implies that melting or at least partial melting of the iPP fiber is in favor of the formation of β-iPP in the fiber/matrix interfacial layer. Therefore, as expected, interfacial layers composed of purely β-iPP crystals were obtained when the fibers were introduced into the matrix melt at their nominal melting point, see Fig. 20.

SEM observations provide further evidence for the occurrence of fiber melting and illustrate the growth process of β-iPP crystalline lamellae [199]. As shown in Fig. 21b, the fiber consists of edge-on lamellae with most of them well arranged in the direction perpendicular to the fiber axis. A few of the iPP lamellae aligned more or less in the axial direction of the fiber, as indicated by a small white arrow, indicates the occurrence of the unique lamellar branching of α-iPP. All these should result from the melting and recrystallization of iPP fiber during sample preparation. Parts c and d of Fig. 21 provide detailed structural information about β-iPP crystal growth at initial stage. It can be seen that the growth of β-iPP crystals starts from several single lamella embedded in the rich α-iPP lamellar region, as indicated by the white arrows. At the early stage, the β-iPP lamellae are loosely packed with some α-iPP inclusion, as indicated by the ellipses. These α- and β-lamellae propagate for few micrometers without interference. Subsequently, the β-iPP lamellae start to branch and splay out leading to the formation of fan-shaped structures, which stop the growth of α-iPP crystals, and finally pure β-iPP crystalline lamellae are observed with non-periodic cracks as indicated by white arrows (Fig. 21e). Further propagation of the β-iPP crystals results in the occurrence of the typical lamellae twisting, see Fig. 21f.

The single fiber induced crystallization of iPP indicates that melt recrystallization of the iPP fiber is in favor of initiating β crystallization of the matrix. It is, however, uncertain whether this is caused by orientation-induced recrystallization or shear-induced crystallization caused by fiber introduction. The result of β recrystallization of the neat molten α-iPP fibers helps to exclude the possibility of shear-induced crystallization. Also the crystallization of iPP matrix in the heterogeneous PET/iPP fiber/matrix system prepared in exactly the same way as the single polymer composite confirms that the β-iPP crystallization in the single polymer composite originates from the oriented iPP chain segments in the molten fiber [201]. As presented in Fig. 22, by introducing the PET fiber into the iPP matrix at 170 °C and then crystallized isothermally at 130 °C for 90 min (Fig. 22a), well-developed column structures of iPP in α-modification surrounding the PET fiber are observed. On the contrary, β-iPP column structures become the solely observed interfacial morphology along the whole PET fiber when introducing PET fiber into the supercooled iPP matrix at temperatures below 150 °C, see Fig. 22b. This is totally different from the case of single iPP fiber/matrix system, and therefore reflects a different crystallization mechanisms of iPP around the PET fiber compared with iPP fiber induced crystallization. It is confirmed that PET fiber exhibits only a

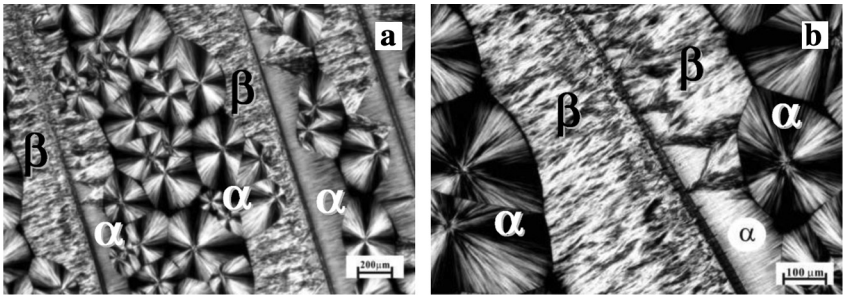

Fig. 19. Optical micrographs of an iPP single-polymer composite with α and β iPP crystals indicated. The fiber introduction temperature was 168 °C and the isothermal crystallization temperature was 138 °C. Reproduced with permission from Ref. [195], copyright© 2003, American Chemical Society.

Fig. 20. Optical micrographs show the morphologies of an iPP fiber/matrix single polymer composite. The fiber introduction temperature was 173 °C. The crystallization temperature was 138 °C. Reproduced with permission from Ref. [195], copyright© 2003, American Chemical Society.

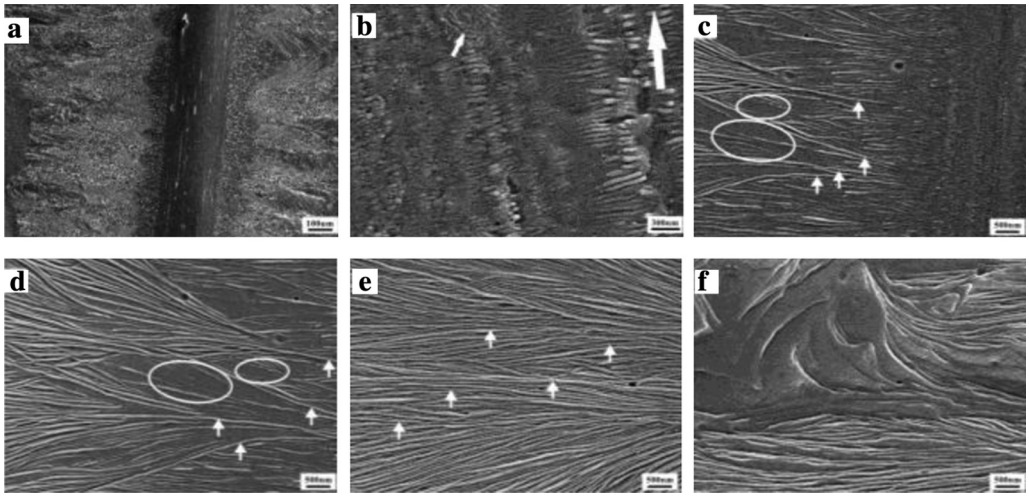

Fig. 21. SEM micrographs of an iPP fiber/matrix single polymer composite prepared by introducing the iPP fiber into its supercooled homogeneity matrix at 168 °C and isothermally crystallized at 135 °C for 1 h. (a) An overall view at low magnification. (b) Surface lamellar structure of the iPP fiber with its axis being indicated by a big white arrow; a small white arrow labels the crosshatched lamellar structure. (c) Interfacial structure with the β-iPP lamellae indicated by white arrows. (d) Growth of β-iPP at early stage. (e) Continuous growth of edge-on β-iPP lamellae with the nonperiodic cracks being indicated by white arrows. (f) Twisting of the β-iPP lamellae. Reproduced with permission from Ref. [199], copyright© 2004, American Chemical Society.

weak α nucleating capacity toward iPP in the quiescent condition [66,70,201,207]. In this case, the influence of sample preparation procedure on the crystallization of iPP overwhelms the heterogeneous nucleation of iPP on the surface of PET fiber. The influence of sample preparation procedure on the crystallization of iPP can be easily removed by keeping the sample at the fiber introduction temperature for a certain period of time. To find out the validity of the above hypothesis, another experiment was performed with the PET fiber being introduced into the supercooled iPP melt at 145 °C, then kept at this temperature for different time and finally moved to another hot plate at 130 °C for isothermal crystallization. As shown in Fig. 23a, a 5 s placement of the sample at 145 °C before crystallization shows no evident effect on the interfacial morphology compared with that formed by direct cooling. A 30 s placement of the sample at 145 °C, as shown in Fig. 23b, leads to the formation of well developed β-iPP column layers with some triangular α-iPP crystals as indicated by white arrows in the picture. When the sample was kept at 145 °C for 10 min, see Fig. 23c, the cylindrites are composed of purely α-iPP crystals. This reveals that the initial state of the melt influences the crystallization of β-iPP in the PET/PP system.

The iPP single polymer system follows another scenario. The existence of perfect lattice matching between the fiber and matrix encourages the occurrence of polymer homoepitaxy. The homoepitaxy is found to be quite efficient in improving the crystallization kinetics of a polymer [208]. Moreover, the better surface wettability of the iPP matrix on its own fiber will also enhance the adsorbability of iPP chains on the surface of the solid fiber and accelerate the secondary nucleation of the iPP chain on its homogenous fiber. All those have enabled a very high nucleation ability of iPP fiber toward its homogeneous matrix. Consequently, the homoepitaxial crystallization of iPP on the solid surface of its highly oriented single polymer fiber caused by heterogeneous nucleation (or secondary nucleation) overwhelms the effect of fiber introduction. As a result, transcrystallization of iPP in its α-form driven by the homoepitaxial crystallization is generated at low fiber introduction temperature since lattice matching possesses a very strong controlling power on the crystal structure of the epitaxial polymer [209–214]. On the other hand, if the iPP fiber was to some extent molten during fiber introduction at high temperature, the molten iPP fiber would not relax much due to the high viscosity and short fiber introduction time (about tens of second). The surviving extended iPP chains or chain segments will serve as self-nuclei and quickly induce the oriented recrystallization of the matrix during the subsequent cooling process [43,44,46,56,215–217].

From the above discussion, the chain orientation status in molten iPP fiber is expected to play an important role in producing β-iPP crystallization. The results obtained from iPP fiber/matrix single polymer composites with iPP fibers of varying molecular weight show indeed different induced crystallization behavior owing to the different relaxation of molecular chains [196]. Fig. 24 shows three representative optical micrographs of iPP single

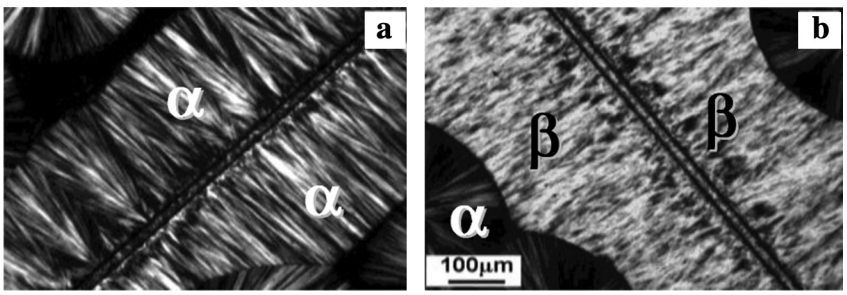

Fig. 22. Optical micrographs of iPP/PET composites, which were prepared by introducing the PET into the supercooled iPP melt at (a) 170 °C and (b) 150 °C, respectively. The isothermal crystallization of the samples were performed at 130 °C for 90 min. Reproduced with permission from Ref. [201], copyright© 2007, American Chemical Society.

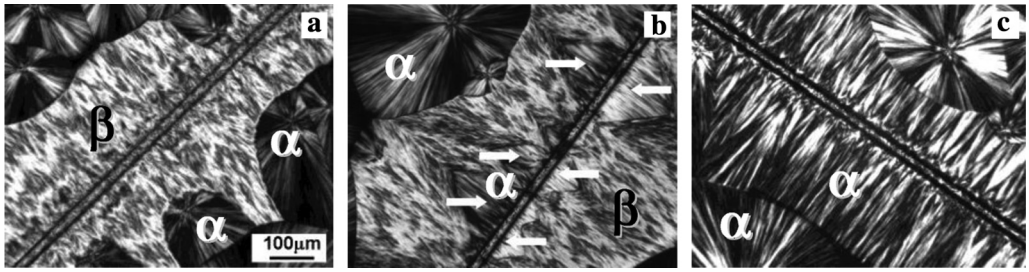

Fig. 23. Optical micrographs of iPP/PET composites. The PET fiber introduction temperature was 145 °C. After fiber introduction, the samples were kept at 145 °C for (a) 5 s, (b) 30 s, and (c) 10 min and then cooled to 130 °C for isothermal crystallization. Reproduced with permission from Ref. [201], copyright© 2007, American Chemical Society.

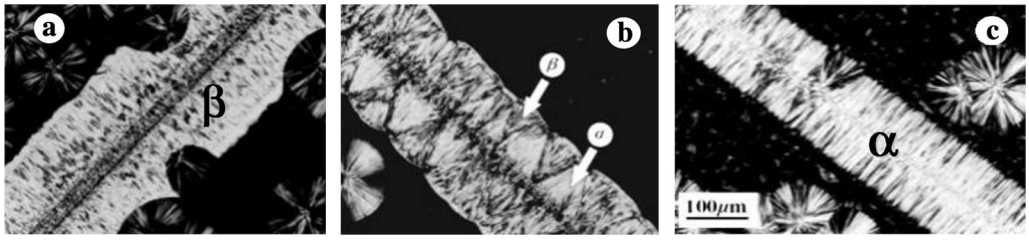

Fig. 24. Optical micrographs of iPP fiber/matrix single polymer composites. The iPP fibers with molecular weight (a) 1.94×10^5, (b) 1.85×10^5 and (c) 1.15×10^5 were introduced into the same iPP melts at (a) 178 °C, (b) 168 °C and (c) 165 °C. The samples were isothermally crystallized at 135 °C. Reproduced with permission from Ref. [196], copyright© 2006, American Chemical Society.

polymer composites with same matrix material and crystallization temperature but different iPP fibers in molecular weight. For high molecular weight fiber system, see Fig. 24a, pure β-iPP crystalline interfacial layers can be produced in a wide temperature range near its nominal melting point. On the contrary, in the sample with low molecular weight fiber, see Fig. 24c, only α-iPP crystalline interfacial layers have been observed at all chosen temperatures. Interfacial morphologies with coexistence of both α- and β-iPP crystals were always observed for the systems with the iPP fibers having moderate molecular weights, see Fig. 24b. These discrepant interfacial morphologies should originate from the different relaxation behavior of the used fibers, which depends strongly on the molecular weight [216,217]. The following equivalent experiments have confirmed the validity of the above conclusion. Fig. 25 shows the optical micrographs of the iPP matrix/fiber (same as that used in Fig. 24a) samples prepared by introducing the fiber into the matrix at 175 °C. After holding at 175 °C for different times, the samples were subsequently cooled to 135 °C for isothermal crystallization. It can be seen that a 5 min maintenance of the sample at 175 °C after fiber introduction (Fig. 25a) induces still the crystallization of iPP in its β-form. Holding the sample at 175 °C for 10 min, not only the total nucleation ability but also the ability in generating β-iPP crystals have decreased obviously, see Fig. 25b. For a 15 min placement of the sample at 175 °C, see Fig. 25c, the nuclei formed along the molten fiber becomes sparse. Individual nucleus along the iPP fiber is now recognizable. Moreover, the appearance of fully α-iPP crystals indicates undoubtedly that the more relaxed molten iPP fiber has lost its ability in triggering its β-crystallization. These experimental results indicate that the relaxation extent of the originally highly oriented iPP chains in the molten iPP fiber is an important parameter for controlling the formation of β-iPP transcrystalline layers. This leads to the conclusion that the formation of β-crystals is associated with the oriented or stretched macromolecular chains survived during incomplete melting of the highly oriented iPP fiber. From this point of view, the melting and recrystallization process of the iPP fiber should be concerned to get a better understanding of the orientation-induced β-iPP crystallization.

The effect of molecular mass of iPP matrix on the crystallization of β-iPP was also studied by introducing iPP fibers with $M_w = 1.94 \times 10^5$ g/mol and draw ratio = 4 into the matrixes with different molecular weight [200]. As shown in Fig. 26a, it is found that β-cylindrites formed around the fiber in the matrix with $M_w = 1.94 \times 10^5$ g/mol. On the other hand, the interfacial morphology for the matrix with $M_w = 4.46 \times 10^5$ g/mol consists of mainly α-crystals (Fig. 26b). There are a few of fan-shaped β-iPP regions (indicated by the arrows). It has to be noted that both iPP matrixes can crystallize in β-form at the existence of β-nucleating

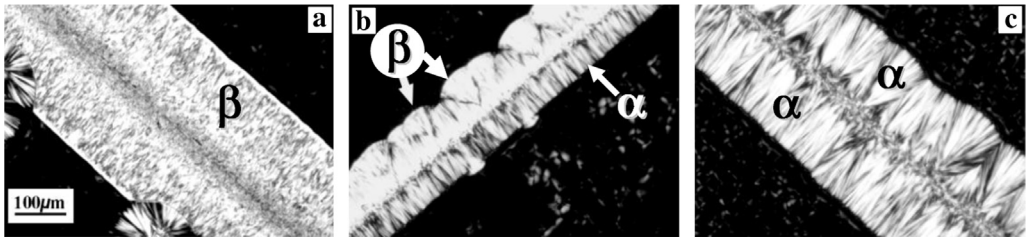

Fig. 25. Optical micrographs of iPP fiber/matrix single polymer composites. The iPP fibers with molecular weight of 1.94×10^5 were introduced into iPP melts at 175 °C, then kept at that temperature for (a) 5, (b) 10, and (c) 15 min and finally cooled to 135 °C for isothermal crystallization. Reproduced with permission from Ref. [196], copyright© 2006, American Chemical Society.

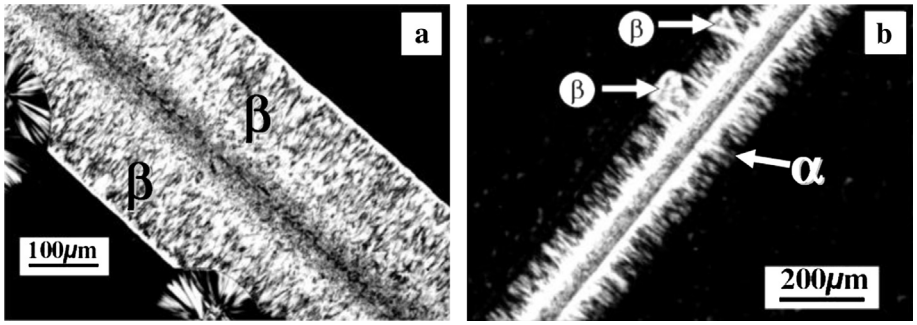

Fig. 26. Optical micrographs of the iPP fiber/matrix composites prepared by introducing the same iPP fiber into molten iPP matrix with molecular weight (a) $M_w = 1.94 \times 10^5$ and (b) $M_w = 4.46 \times 10^5$ at 180 °C and subsequently isothermally crystallized at 138 °C for 2 h. Reproduced with permission from Ref. [200], copyright© 2006, American Chemical Society.

agent. This indicates that the iPP chains in the matrix participate in the nucleation process of β-iPP. A phenomenological hypothesis for the nucleation of the β-phase is that the necessary condition for the formation of β-nuclei requires the participation of iPP chains in the matrix with the oriented iPP chains at the partially relaxed fiber surface. In this case, some extent of iPP chain relaxation at the fiber surface is necessary for the penetration of the matrix chains. The chain orientation of iPP in the molten fiber should also maintain above a critical level for creating β-nuclei. Lacking such relaxation and interdiffusion, the solid fiber surface will act as a substrate for homoepitaxy of the α-phase. Considering that the diffusivity is inversely proportional to the square of the molecular mass [218,219], the diffusivity of matrix with $M_w = 1.94 \times 10^5$ is estimated ca. 5 times greater than that of the matrix with $M_w = 4.46 \times 10^5$. Therefore, the required chain interpenetration and relaxation for β-nucleation could be easily realized in the lower molecular weight matrix.

It is well known that the melting behavior of macromolecules is different from that of the low molecular weight compounds. Due to the long chain character, the macromolecular chains should experience a "recoiling" or "relaxation" process during melting. The recoiling process may take quite long time depending on melting temperature and the molecular weight. Extensive studies on the relaxation and crystallization of sheared polymer melt indicated that metastable oriented structures in sheared polymer melt might resist relaxation upon cessation of shearing and could act as "prenuclei" from which fold chain lamellae grow with the chain axis highly oriented along the shear direction [43,44,46,215]. These "prenuclei" can remain active only for a certain period of time after cessation of shear flow at the temperatures above its melting point. Azzurri and Alfonso reported that the lifetime of the nucleation precursors is very sensitive to both relaxation temperature and molecular weight [216,217]. The melting and recrystallization processes of highly oriented iPP fiber are actually similar to the sheared iPP melt. Considering that the fiber introduction was performed in a quite short time and at temperatures close to or slightly above its nominal melting point, a complete recoiling of the molten iPP fiber could hardly be attained before recooling of the samples. Varga et al. [56] found that some local order of the molecular chains previously included in a crystal lattice could be preserved as "prenuclei" or sometime referred to "nucleation precursors" through studying the effect of melting history on the recrystallization of iPP by optical microscopy. Taking this into account, one may argue that the partially or incompletely molten iPP fibers exist actually in the form of amorphous domains with oriented or stretched macromolecular chain segments as in the sheared melt. These oriented molecular segments or chains, in turn, serve as nucleation precursors and initiate the β-iPP crystallization during cooling process just like the case of shear-induced crystallization. Selective melting of the β-crystals displays, however, a scenario different from the shear-induced iPP crystallization by fiber pulling.

Fig. 27 shows the optical micrographs of an iPP single polymer composite before and after melting of the β-iPP crystals. In the interface layer, some randomly dispersed leaf-shaped α-iPP inclusions are clearly visible. Comparing parts a and b of Fig. 27, one may notice that a transition of α-iPP spherulites from mixed type (α_m) into negative radial type (α_{II}) has been realized by annealing at 158 °C for a short time [68]. From Fig. 27b, the similar diameter and relatively smooth surface of the recrystallized iPP fiber compared with the used original one implies that the growth of the β-iPP transcrystals starts directly from the fiber surface. This is different from what observed in heterogeneous fiber/matrix composites produced by fiber pulling, where α-iPP layers with zigzag edges on both sides of the heterogeneity fiber were observed after melting of the β-iPP cylindrites. Moreover, it was occasionally observed that the iPP fibers could be broken off by selective melting at

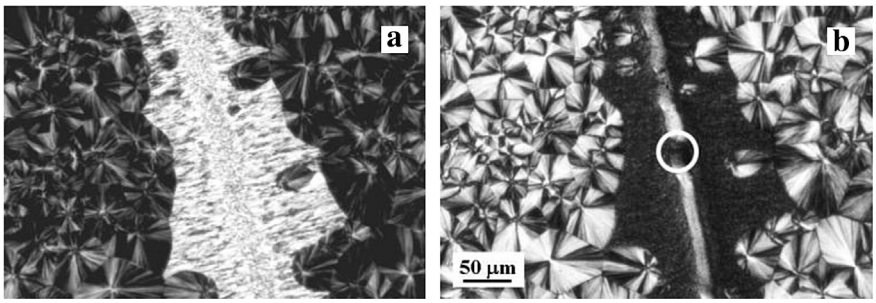

Fig. 27. Polarized optical micrographs of an iPP fiber/matrix composite crystallized isothermally at 116 °C for 30 min. The temperature of fiber introduction was 173 °C. (a) As-prepared sample and (b) After melting of the β-iPP crystals at 158 °C. Reproduced with permission from Ref. [196], copyright© 2006, American Chemical Society.

temperatures above the melting point of β-iPP but below that of α-iPP, see the circled part in Fig. 27b. Since the used iPP fibers are originally in their α-form, the breakage of the iPP fiber unambiguously implies that some local parts of the original α-iPP fiber have transformed into β-form through melting and recrystallization. From this point, one may conclude that the melting status, or in other words, the degree of local chain orientation of the molten iPP fiber plays a very important role in generating transcrystalline β-iPP crystals. This has been further confirmed by fiber pulling experiments with controlled pulling rate and time.

It was found that the interfacial morphologies of iPP on Kevlar fibers, which exhibit no nucleation ability to iPP in quiescent melt, could vary from pure α-cylindrites to pure β-cylindrites in the pulled system depending upon fiber pulling rate and duration [202]. At a very low fiber pulling rate of 17 μm/s, the enhanced nucleation ability of the fiber to the iPP matrix leads to the formation of α-iPP cylindrites and indicates the existence of shear exerted on the iPP melt. As in the steady shear-experiments, an increase of β-iPP content was seen at high fiber-pulling rate with increasing pulling time. These results indicate that a certain extent of chain orientation is required to initiate β-crystallization of iPP, or the existence of a lower threshold of chain orientation for initiating β-crystallization of iPP. Therefore, at lower fiber pulling rate, since chain orientation and relaxation take place simultaneously during fiber pulling, the iPP chains in the molten state can hardly be oriented well enough for triggering β-crystallization of iPP. At higher fiber pulling rate, chain orientation is faster than relaxation and high degree of chain orientation for initiating β-iPP crystallization can be achieved in a short time. From this viewpoint, it is expected to obtain pure β-iPP crystals at appropriate shear conditions in steady state shear experiments. This is, however, never realized. On the contrary, a reduction in the β-iPP crystal content was seen with further increase of the shear rate [191]. This result implies the existence of an upper threshold of chain orientation for β-iPP crystallization, which is confirmed by our selective melting experiments. Fig. 28a and b show the optical micrographs of samples prepared by pulling the fibers at 131 °C along the fiber axis at different pulling rate for different duration, and then isothermally crystallized for sufficient time. It can be seen that β-iPP cylindrites are produced in both cases. After selective melting of the β-iPP crystals at 158 °C, the morphologies of the remaining α-iPP crystals are quite interesting. As shown in parts c and d of Fig. 28, while smooth fiber surface is seen at lower fiber pulling rate, residual α-iPP crystal layers surrounding the fiber have been observed at higher fiber pulling rate. This indicates that a better chain orientation of the iPP directly in contact with the fiber achieved at higher fiber pulling rate leads to the formation of thin α-iPP transcrystalline layers around the fiber. From the above discussion, it is concluded that there exists a chain orientation window, in which nucleation of β-iPP crystals is preferred. As a result, poor chain orientation outside of this window results in only α-iPP cylindrites, while highly oriented molecular chains beyond this window initiate first the oriented α-iPP crystals and then the β-iPP crystals. This may be the reason for the formation of oriented α-iPP crystals in melt-drawn thin film (Fig. 8) and the α-iPP shish-kebab structure shown in Fig. 11.

Combing the results presented in this section, it was found that a higher crystal growth rate of β-iPP compared with its α-counterpart is a necessary condition for β-iPP crystallization. Otherwise the fast growing α-iPP crystals will embed the generated β-nuclei. The local order and environment of the macromolecular chains just before nucleation are important for β-nucleation of iPP. It seems that the formation of β-iPP nuclei is restricted in a certain chain orientation window of the iPP melt. At presented stage, the exact

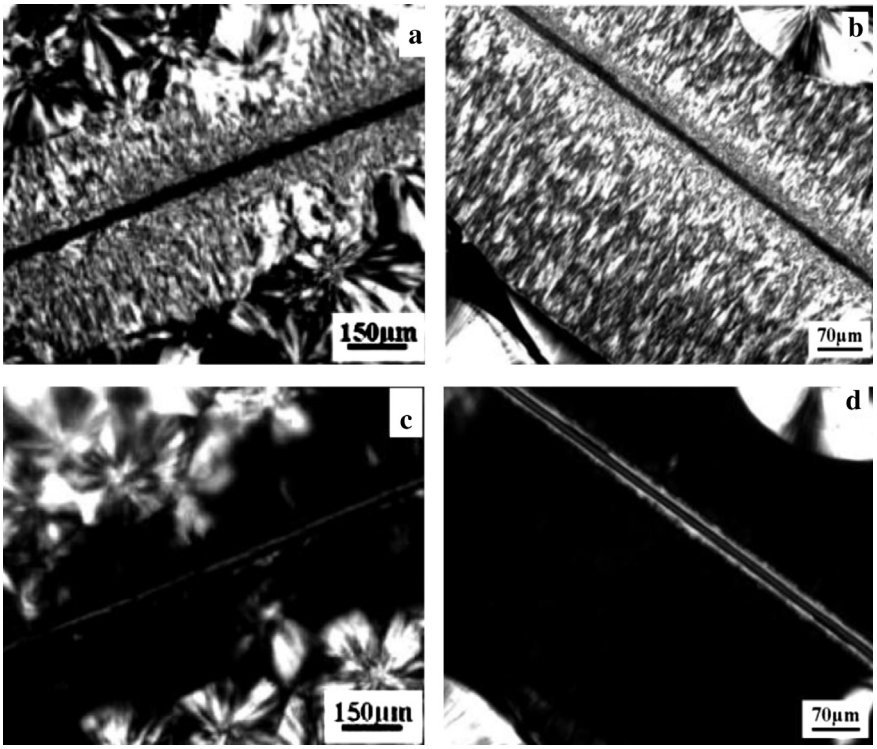

Fig. 28. Optical micrographs present the interface morphologies of the iPP/Kevlar matrix/fiber systems. The samples were heat-treated at 210 °C for 5 min and then quickly cooled to and kept at 131 °C for fiber pulling and isothermal crystallization. The fibers were pulled (a) at a rate of 40 m/s for 10 s and (b) at a rate of 515 m/s for 1 s. Parts c and d highlight the morphologies of the residual α-crystals after selective melting of the β-iPP crystals at 158 °C of the samples shown in a and b, respectively. Reproduced with permission from Ref. [202], copyright© 2006, American Chemical Society.

origin of the nucleation process of β-iPP is not quite clear. Considering that isochiral chains are involved in the β-iPP crystals, one may suggest that microdomains with isochiral chains are probably produced through chains rotation in the viscous melt during relaxation. These isochiral chain aggregates transform into β-iPP nuclei during cooling process and initiate the growth of β-iPP crystals. Further experimental and simulation work are needed to clarify this.

6. Concluding remarks

During polymer processing, the polymer melts are frequently subjected to shear or/and elongation flow fields, which produce molecular chain orientation in the melt. The oriented molecular chains crystallized in a different way as that encountered under quiescent conditions. Therefore, the orientation-induced crystallization has long been an object of intense interests. This leads to a vast body of researches about the effects of preorientation on the crystallization of various polymers. Among them, iPP is most frequently studied since its diversified structure and morphology are very sensitive not only to the changes in processing conditions but also to its molecular parameters. For example, depending on different molecular structure and thermal and mechanical treatments, three different crystalline structures, i.e. the monoclinic α, the hexagonal β and the orthorhombic γ, can be produced. It was well demonstrated that a sheared or strained melt encouraged the β-crystallization of iPP. Taking this into account, the study on orientation-induced crystallization is also expected to be helpful for a better understanding of the β-iPP crystallization.

Systematical studies on the crystallization kinetics of iPP under flow field, which produces oriented or even stretched molecular chains, show that the crystallization process is affected remarkably by the preorientation of the molecular chains. This is manifested by an evident enhancement in the overall crystallization rates. As an example, it is found that a change of a factor of 2 in the imposed shear rate ($\dot{\gamma}$) could result in a ten-fold increase in the crystallization rate of iPP. First of all, flow affects the crystal growth speed. This rests on the fact that the organization of preordered polymer chain segments into the crystal lattice rather easily since they are to some extent closer to their state in the crystal phase, which exhibit a less kinetic barrier to overcome compared with the random coiled chains. The contribution of crystal growth to enhanced overall global kinetics is, however, rather limited as compared with the significant acceleration of nucleation. It was widely accepted that the effect of flow on polymer crystallization is mainly in the change of the nucleation process and the nucleation density. This is well supported by the experimental results obtained from the earliest stage of crystallization process under flow. It is also well explained theoretically under the help of phenomenological models. Actually, the proposed theoretic model can be used not only to explain the observed experimental phenomena qualitatively but also to predict the influence of flow on crystallization kinetics precisely.

Studies on the final morphology of iPP indicate that shear flow encourages the formation of highly oriented structures. At appropriate conditions, shish-kebab structures have been observed even at a low shear rate. It is found that the iPP molecular chains undergo a sharp transition from random coil to an extended-chain conformation under flow, i.e., coil–stretch transition. The stretched molecular chains form extended chain "shish" crystals, which initiate the overgrowth of folded chain "kebab" crystals. Many experimental results suggested that the shear-induced iPP shish crystals may involve a large number of entangled molecules. It is somewhat different from the traditional scenario about the shish-kebab structures. Therefore, new models about the shear-induced shish-kebab structure of iPP have been proposed based on the new experimental results. A fully understanding about this aspect should be one of the most important challenges in this field.

Studies on the crystal structure of iPP obtained from its preoriented melt indicate that both α and β iPP crystals can be produced depending on the orientation status and crystallization conditions. It is found that a faster β-iPP crystal growth rate is necessary but not sufficient for promoting β-iPP crystallization, or in other words, the formation of β-iPP crystalline nuclei is the prerequisite for β-iPP crystallization. Based on the recent experimental results, it is suggested that the formation of the β-iPP nuclei may be restricted in a certain chain orientation window of the iPP melts. Poorly oriented iPP chains in the melt crystallize in the α-iPP form cylindrites, while highly oriented molecular iPP chains beyond this window initiate first the oriented α-iPP crystals and then β-iPP crystals. At presented stage, the exact origin of the β-iPP nucleation process is not quite clear. A better understanding of the orientation-induced β-iPP crystallization should be another challenge of this field.

Acknowledgments

A portion of the used materials is based on the researches supported by the National Natural Science Foundation of China under Grant No. 50833006, 21274009, 51221002 and 50973008.

References

[1] Odell JA, Grubb DT, Keller A. Polymer 1978;19:617.
[2] Bushman AC, McHugh AJ. J Appl Polym Sci 1997;64:2165.
[3] Okamoto M, Kubo H, Kotaka T. Macromolecules 1998;31:4223.
[4] Jay F, Haudin JM, Monasse B. J Mater Sci 1999;34:2089.
[5] Eder G, Janeschitz-Kriegl H. In: Meijer HEH, editor. Materials science and technology, vol. 18. Weinheim: Verlag Chemie; 1997. p. 269.
[6] Duplay C, Monasse B, Haudin JM, Costa JL. J Mater Sci 2000;35:6093.
[7] Abuzaina FM, Fitz BD, Andjelić S, Jamiolkowski DD. Polymer 2002;43:4699.
[8] Kumaraswamy G, Issaian AM, Kornfield JA. Macromolecules 1999;32:7537.
[9] Varga J. Angew Makromol Chem 1983;112:191.
[10] Varga J, Karger-Kocsis J. J Polym Sci Part B: Polym Phys 1996;34:657.
[11] Wu CM, Chen M, Karger-Kocsis J. Polymer 1999;40:4195.
[12] Gahleitner M, Wolfschwenger J, Bachner C, Bernreitner K, Neissl W. J Appl Polym Sci 1996;61:649.
[13] Huang HX. J Appl Polym Sci 1998;67:2111.
[14] Kalay G, Bevis MJ. J Polym Sci Part B: Polym Phys 1997;35:265.
[15] Wilkinson AN, Ryan AJ. Polymer processing and structure development. Dodrecht: Academic Publishers; 1998. p. 1.
[16] Haas TW, Maxwell B. Polym Eng Sci 1969;9:225.
[17] Wereta A, Gogos C. Polym Eng Sci 1971;11:19.
[18] Lagasse RR, Maxwell B. Polym Eng Sci 1976;16:189.
[19] Monasse B. J Mater Sci 1995;30:5002.
[20] Tribout C, Monasse B, Haudin JM. Colloid Polym Sci 1996;274:197.
[21] Kobayashi K, Nagasawa T. J Macromol Sci Phys B 1970;4:331.
[22] Krueger D, Yeh GSY. J Appl Phys 1972;43:4339.
[23] Fritzsche AK, Price FP. Polym Eng Sci 1974;14:401.
[24] Fritzsche AK, Price FP, Ulrich RD. Polym Eng Sci 1976;16:182.
[25] Andersen PG, Carr SH. Polym Eng Sci 1978;18:215.
[26] Sherwood CH, Price FP, Stein RS. J Polym Sci Polym Symp 1978;63:77.
[27] Wolkowicz MD. J Polym Sci Polym Symp 1978;63:365.
[28] Tan V, Gogos CG. Polym Eng Sci 1976;16:512.
[29] Liedauer S, Eder G, Janeschitz-kriegl H, Jerschow P, Geymayer W, Ingolic E. Int Polym Process 1993;8:236.
[30] Monasse B. J Mater Sci 1992;27:6047.
[31] Devaux E, Chabert B. Polym Commun 1991;32:464.
[32] Chabert B, Chauchard J. Ann Chim Fr 1991;16:173.
[33] Thomason JL, van Rooyen AA. J Mater Sci 1992;27:897.
[34] Varga J, Karger-Kocsis J. Composites Sci Technol 1993;48:191.
[35] Misra A, Deopura BL, Xavier SF, Hartley FD, Peters RH. Angew Makromol Chem 1983;113:113.
[36] Liedauer S, Eder G, Janeschitz-kriegl H. Int Polym Process 1995;10:243.
[37] Jerschow P, Janeschitz-Kriegl H. Int Polym Process 1997;12:72.
[38] Jerschow P, Janeschitz-Kriegl H. Rheol Acta 1996;35:127.
[39] Kumaraswamy G, Verma RK, Kornfield JA. Rev Sci Instrum 1999;70:2097.
[40] Peterlin A. Colloid Polym Sci 1987;265:357.

[41] Somani RH, Yang L, Zhu L, Hsiao BS. Polymer 2005;46:8587.
[42] Zhu PW, Edward G. Macromol Mater Eng 2003;288:301.
[43] Somani RH, Hsiao BS, Nogales A, Srinivas S, Tsou AH, Sics I, et al. Macromolecules 2000;33:9385.
[44] Somani RH, Hsiao BS, Nogales A, Fruitwala H, Srinivas S, Tsou AH. Macromolecules 2001;34:5902.
[45] Somani RH, Yang L, Sics I, Hsiao BS, Pogodina NV, Winter HH, et al. Macromol Symp 2002;185:105.
[46] Nogales A, Hsiao BS, Somani RH, Srinivas S, Tsou AH, Balta-Calleja FJ, et al. Polymer 2001;42:5247.
[47] Moitzi J, Skalicky P. Polymer 1993;34:3168.
[48] Pople JA, Mitchell GR, Chai CK. Polymer 1996;37:4187.
[49] Pople JA, Mitchell GR, Sutton SJ, Vaughan AS, Chai CK. Polymer 1999;40:2769.
[50] Goschel U, Swartjes FHM, Peters GWM, Meijer HEH. Polymer 2000;41:1541.
[51] Pogodina NV, Lavrenko VP, Srinivas S, Winter HH. Polymer 2001;42:9031.
[52] Duplay C, Monasse B, Haudin JM, Costa JL. Polym Int 1999;48:320.
[53] Seki M, Thurman DW, Oberhauser JP, Kornfield JA. Macromolecules 2002;35:2583.
[54] Koscher E, Fulchiron R. Polymer 2002;43:6931.
[55] Elmoumni A, Winter HH, Waddon AJ, Fruitwala H. Macromolecules 2003;36:6453.
[56] Varga J. J Mater Sci 1992;27:2557.
[57] Keller A, Kolnaar HWH. Processing of polymers, vol. 18. New York: Wiley-VCH; 1997. p. 189.
[58] Wunderlich B. Macromolecular physics. New York: Academic Press; 1973.
[59] Ryan AJ, Terrill NJ, Fairclough JPA. ACS Symp Ser 2000;739:201.
[60] Mitchell GR, Holt JJ, Thornley SA, Chai CK. Proceedings of the international conference on flow-induced crystallization of polymers – impact to proceeding and manufacture properties. Italy: Salerno; 2001. p. 15.
[61] Salerno, Italy. Alfonso GC, Azzurri F, editors. Proceeding of the international conference on flow induced crystallization of polymers 2001. p. 27.
[62] Bassett DC. Proceedings of the international conference on flow-induced crystallization of polymers – impact to proceeding and manufacture properties. Salerno, Italy; 2001. p. 59.
[63] Keller A, Machin MJ. J Macromol Sci B 1967;1:41.
[64] Kumaraswamy G, Verma RK, Issaian AM, Wang P, Kornfield JA, Yeh F, et al. Polymer 2000;41:8931.
[65] Varga J, Karger-Kocsis. Polym Bull 1993;30:105.
[66] Varga J, Karger-kocsis J. J Mater Sci Lett 1994;13:1069.
[67] Leugering HJ, Kirsch G. Angew Makromol Chem 1973;33:17.
[68] Varga J, Ehrenstein GW. Polymer 1996;37:5959.
[69] Varga J. J Macromol Sci Phys 2002;B41:1121.
[70] Varga J. In: Karger-Kocsis J, editor. Polypropylene structure blends and composites, vol. 1. London: Chapman & Hall; 1995. p. 56.
[71] Meille SV, Ferro DR, Bruckner S, Lovinger AJ, Padden FJ. Macromolecules 1994;27:2615.
[72] Lotz B, kopp S, Dorset DCR. Acad Sci Paris 1994;319(IIb):187.
[73] Lotz B, Wittmann JC, Lovinger AJ. Polymer 1996;37:4979.
[74] Kornfield JA, Kumaraswamy G, Issaian AM. Ind Eng Chem Res 2002;41:6383.
[75] Coppola S, Grizzuti N, Maffettone PL. Macromolecules 2001;34:5030.
[76] Godara A, Raabe D, Van Puyvelde P, Moldenaers P. Polym Test 2006;25:460.
[77] Elmoumni A, Gonzalez-Ruiz RA, Coughlin EB, Winter HH. Macromol Chem Phys 2005;206:125.
[78] Wassner E, Maier RD. Shear-induced crystallization of polypropylene melts. In: Proceeding of the XIII international congress on rheology 2000. p. 1–183.
[79] Janeschitz-Kriegl H, Ratajski E, Stadlbauer M. Rheol Acta 2003;42:355.
[80] Janeschitz-Kriegl H. Monatshefte Chem 2007;138:327.
[81] Janeschitz-Kriegl H, Eder G. J Macromol Sci Chem 1990;A27(13 & 14):1733.
[82] Eder G, Janeschitz-Kriegl H, Liedauer S. Prog Polym Sci 1990;15:629.
[83] Eder G, Janeschitz-Kriegl H. Mater Sci Technol 1997;18:268.
[84] Nieh J, Lee L. J Polym Eng Sci 1998;38:1121.
[85] White-Bischoff EE, Winter HH, Rothstein JP. Rheol Acta 2012;51:303.
[86] Somani RH, Yang L, Hsiao BS. Polymer 2006;47:5657.
[87] Avila-Orta CA, Burger C, Somani RH, Yang L, Marom G, Medellin-Rodriguez FJ, et al. Polymer 2005;46:8859.
[88] Dikovsky D, Marom G, Avila-Orta CA, Somani RH, Hsiao BS. Polymer 2005;46:3096.
[89] Doufas AK, Dairanieh IS, McHugh AJ. J Rheol 1999;43:85.
[90] McHugh AJ. Polym Eng Sci 1982;22:15.
[91] Zuidema H, Peters GWM, Meijer HEH. Macromol Theory Simul 2001;10:447.
[92] Doufas AK, McHugh AJ, Miller C. J Non-Newtonian Fluid Mech 2000;92:27.
[93] Doufas AK, McHugh AJ, Miller C, Immanemi A. J Non-Newtonian Fluid Mech 2000;92:81.
[94] Ziabicki A, Jarecki L. Ziabicki A, Kawai H, editors. High-speed fiber spinning. New York: Wiley; 1985. p. 225.
[95] Acierno S, Coppola S, Grizzuti N, Maffettone PL. Macromol Symp 2002;185:233.
[96] Coppola S, Balzano L, Gioffredi E, Maffettone PL, Grizzuti N. Polymer 2004;45:3249.
[97] Turnbull D, Fisher JC. J Chem Phys 1949;17:71.
[98] Doi M, Edwards SF. The theory of polymer dynamics. Oxford: Clarendon Press; 1986.
[99] Norton DR, Keller A. Polymer 1985;26:704.
[100] Natta G, Corradini P. Nuovo Cimento Suppl 1960;15:40.
[101] Padden FJ, Keith HD. J Appl Phys 1959;30:1479.
[102] Padden FJ, Keith HD. J Appl Phys 1966;37:4013.
[103] Binsbergen FL, De Lange BGM. Polymer 1968;9:23.
[104] Khoury F. J Res Natl Bur Stand Sec A 1966;70A:29.
[105] Lotz B, Wittmann JC. J Polym Sci Part B: Polym Phys 1986;24:1541.
[106] Turner-Jones A, Aizlewood JM, Beckett DR. Makromol Chem 1964;75:134.
[107] Lotz B, Graff S, Wittman JC. J Polym Sci Polym Phy Ed 1986;24:2017.
[108] Wunderlich B. Thermal analysis, vol. 95. London: Academic Press; 1990. p. 32.
[109] Piccarolo S, Saiu M, Brucato V, Titomanlio G. Appl Polym Sci 1992;46:625.
[110] Keith HD, Padden FJ, Walter NM, Wyckoff HW. J Appl Phys 1959;30:1485.
[111] Zhou JJ, Liu JG, Yan SK, Dong JY, Li L, Chan CM, et al. Polymer 2005;46:4077.
[112] Yan S, Katzenberg F, Petermann J. J Polym Sci Phys Ed 1999;37:1893.
[113] Li HH, Sun XL, Wang JJ, Yan SK, Schultz JM. J Polym Sci Part B: Polym Phys 2006;44:1114.
[114] Turner-Jones A, Cobbold AJ. J Polym Sci Polym Lett 1968;6:539.
[115] Corradini P, de Rosa C, Guerra G, Petraccone V. Polym Commun 1989;30:281.
[116] An B. Acta Polymerica Sinica 1993;3:330.
[117] Olley RH, Hodge AM, Bassett DC. J Polym Sci Part B: Polym Phys 1979;17:627.
[118] Olley RH. Sci Prog Oxf 1986;70:17.
[119] Geil PH. Polymer single crystals. New York: Interscience; 1963.
[120] Varga J, Ehrenstein GW. Colloid Polym Sci 1997;275:511.
[121] Varga J, Mudra I, Ehrenstein GW. Morphology and properties of β-nucleated injection molded isotactic polypropylene. In: 'Antec 98' conference proceedings 1998;vol. 3. p. 3492. Atlanta, USA.
[122] Jenckel E, Teege E, Hinrichs W. Kolloid Zeitschrift 1952;129:19.
[123] Binsbergen FL, Kolloid ZZ. Polymer 1970;238:389.
[124] Bruckner S, Meille SV. Nature 1989;340:455.
[125] Turner-Jones A. Polymer 1966;7:23.
[126] Turner-Jones A. Polymer 1971;12:487.
[127] Mezghani K, Phillips PJ. Polymer 1997;38:5725.
[128] Mezghani K, Phillips PJ. Polymer 1998;39:3735.
[129] Brückner S, Meille SV, Petraccone V, Pirozzi B. Prog Polym Sci 1991;16:361.
[130] Alamo RG, Kim M-H, Galante MJ, Isasi JR, Mandelkern L. Macromolecules 1999;32:4050.
[131] Liu B-B, Shangguan Y-G, Zheng Q. Chin J Polym Sci 2012;30:853.
[132] Hosier IL, Alamo RG, Esteso P, Isasi JR, Mandelkern L. Macromolecules 2003;36:5623.
[133] Sobue H, Tabata Y. J Polym Sci 1959;39:427.
[134] Saraf RF, Porter RS. Mol Cryst Liq Cryst Lett 1985;2:85.
[135] Corradini P, Petraccone V, de Rosa C, Guerra G. Macromolecules 1986;19:2699.
[136] Wu Y, Liang X-Y, Chen R-F, Shangguan Y-G, Zheng Q. Chin J Polym Sci 2012;30:470.
[137] Petermann J, Gohil RM. J Mater Sci Lett 1979;14:2260.
[138] Keller A, Kolnaar HW. Mater Sci Technol 1997;18:189.
[139] Keller A, Hikosaka M, Rastogi S, Toda A, Barham PJ, Goldbeck-Wood G. J Mater Sci 1994;29:2579.
[140] Keller A, Cheng SZD. Polymer 1998;39:4461.
[141] Mackley MR, Keller A. Polymer 1973;14:16.
[142] Pope DP, Keller A. Colloid Polym Sci 1978;256:751.
[143] Miles MJ, Keller A. Polymer 1980;21:1295.
[144] Fu BX, Yang L, Somani RH, Zong SX, Hsiao BS, Phillips S, et al. J Polym Sci Part B Polym Phys 2001;39:2727.
[145] Yang L, Somani RH, Sics I, Hsiao BS, Kolb R, Fruitwala H, et al. Macromolecules 2004;37:4845.
[146] Somani RH, Yang L, Hsiao BS, Sun T, Pogodina NV, Lustiger A. Macromolecules 2005;38:1244.
[147] Hsiao BS, Yang L, Somani RH, Avila-Orta CA, Zhu L. Phys Rev Lett 2005;94:117802.
[148] Somani RH, Yang L, Hsiao BS, Agarwal P, Fruitwala H, Tsou AH. Macromolecules 2002;35:9096.
[149] Agarwal PK, Somani RH, Weng W, Mehta A, Yang L, Ran S, et al. Macromolecules 2003;36:5226.
[150] Somani RH, Yang L, Hsiao BS. Physica A 2002;304:145.
[151] Ran S, Zong X, Fang D, Hsiao BS, Chu B, Phillips RA. Macromolecules 2001;34:2569.
[152] Liu C, Muthukumar M. J Chem Phys 1998;109:2536.
[153] Muthukumar M, Welch P. Polymer 2000;41:8833.
[154] Dukovski I, Muthukumar M. J Chem Phys 2003;118:6648.
[155] Zhang CG, Hu HQ, Wang DJ, Yan SK, Han CC. Polymer 2005;46:8157.
[156] Zhang CG, Hu HQ, Wang XH, Yao YH, Dong X, Wang DJ, et al. Polymer 2007;48:1105.
[157] Meng K, Dong X, Zhang XH, Zhang CG, Han CC. Macromol Rapid Commun 2006;27:1677.
[158] Meng K, Dong X, Hong S, Wang X, Cheng H, Han CC. J Chem Phys 2008;128:024906.
[159] Hu W, Frenkel D, Mathot VBF. Macromolecules 2002;35:7172.
[160] Ryan AJ, Stanford JL, Bras W, Nye TMW. Polymer 1997;38:759.
[161] Hobbs JK, Miles MJ. Macromolecules 2001;34:353.
[162] de Gennes PG. J Phys Chem 1974;15:60.
[163] Somani RH, Yang L, Hsiao BS, Fruitwala H. J Macromol Sci Part B: Phys 2003;B42:515.

[164] Perkins TT, Smith DE, Chu S. Science 1997;276:2016.
[165] Pogodina NV, Siddiquee SKS, VanEgmond JW, Winter HH. Macromolecules 1999;32:1167.
[166] Pogodina NV, Winter HH. Macromolecules 1998;31:8164.
[167] Karger-Kocsis J, Moos E, Mudra I, Varga J. J Macromol Sci Part B: Phys 1999;38:645.
[168] Karger-Kocsis J. Polym Eng Sci 1996;36:203.
[169] Huang M, Li XG, Fang BR. J Appl Polym Sci 1995;56:1323.
[170] Lovinger AJ, Chua JO, Gryte CC. J Polym Sci Polym Phys Ed 1977;15:641.
[171] Lovinger AJ. J Polym Sci Polym Phys 1983;21:97.
[172] Fujiwara Y. Colloid Polym Sci 1975;253:273.
[173] Marco C, Gómez MA, Ellis G, Arribas JM. J Appl Polym Sci 2002;86:531.
[174] Dong M, Jia M-Y, Guo Z-X, Yu J. Chin J Polym Sci 2011;29:308.
[175] Shi G, Zhang J. Chin Sci Bull 1980;12:731.
[176] Feng J, Chen M, Huang Z. Chem J Chin Univ 2001;22:154.
[177] Cho K, Saheb DN, Yang H, Kang B, Kim J, Lee S. Polymer 2003;44:4053.
[178] Chen HB, Karger-Kocsis J, Wu JS, Varga J. Polymer 2002;43:6505.
[179] Cho K, Saheb DN, Choi J, Yang H. Polymer 2002;43:1407.
[180] Feng J, Chen M. Polym Int 2003;52:42.
[181] Zhou G, He Z, Yu J, Han Z, Shi G. Macromol Chem 1986;187:633.
[182] Varga J. J Therm Anal 1989;35:1891.
[183] Mathieu C, Thierry A, Wittmann JC, Lotz B. J Polym Sci Part B: Polym Phys 2002;40:2504.
[184] Varga J, Mudra I, Ehernstein GW. J Appl Polym Sci 1999;74:2357.
[185] Stocker W, Schumacher M, Graff S, Thierry A, Wittmann JC, Lotz B. Macromolecules 1998;31:807.
[186] Assouline E, Pohl S, Fulchiron R, Grard JF, Lustiger A, Wagner HD, et al. Polymer 2000;41:7843.
[187] Dorset DL, McCourt MP, Kopp S, Schumacher M, Okihara T, Lotz B. Polymer 1998;39:6331.
[188] Varga J, Mudra I, Ehrenstein GW. J Thermal Anal Calorim 1999;56:1047.
[189] Hubeny H, Muschik H. J Polym Sci Polym Phys 1977;15:1779.
[190] Somani RH, Sics I, Hsiao BS. J Polym Sci Part B: Polym Phys 2006;44:3553.
[191] Huo H, Jiang SC, An LJ. Macromolecules 2004;37:2478.
[192] Varga J, Karger-kocsis J. Polymer 1995;36:4877.
[193] Varga J, Fujiwara Y, Ille A. Periodica Polytech Chem Eng 1990;34:255.
[194] Shi GY, Zhang XD, Qiu ZX. Makromol Chem 1992;193:583.
[195] Li HH, Jiang SD, Wang JJ, Wang DJ, Yan SK. Macromolecules 2003;36:2802.
[196] Sun XL, Li HH, Zhang X, Wang JJ, Wang DJ, Yan SK. Macromolecules 2006;39:1087.
[197] Li HH, Zhang XQ, Duan YX, Wang DJ, Li L, Yan SK. Polymer 2004;45:8059.
[198] Li HH, Liu JC, Wang DJ, Yan SK. Colloid Polym Sci 2003;281:601.
[199] Li H, Zhang X, Kuang X, Wang J, Wang D, Li L, et al. Macromolecules 2004;37:2847.
[200] Sun XL, Li HH, Zhang XQ, Wang DJ, Schultz JM, Yan SK. Macromolecules 2010;43:561.
[201] Sun XL, Li HH, Lieberwirth I, Yan SK. Macromolecules 2007;40:8244.
[202] Sun X, Li H, Wang D, Yan S. Macromolecules 2006;39:8720.
[203] Li HH, Sun XL, Yan SK, Schultz JM. Macromolecules 2008;41:5062.
[204] Loos J, Schimanski T, Hoffman J, Peijs T, Lemstra PJ. Polymer 2001;42:3827.
[205] Padden Jr FJ, Keith HD. J Appl Phys 1973;44:1217.
[206] Lotz BJ. Macromol Sci 2002;B41:685.
[207] Folkes MJ, Hardwick ST. J Mater Sci Lett 1984;3:1071.
[208] Liu J, Wang JJ, Li HH, Shen DY, Zhang JM, Ozaki Y, et al. J Phys Chem B 2006;110:738.
[209] Lovinger AJ. Polymer 1981;22:412.
[210] Wittmann JC, Lotz B. Prog Polym Sci 1990;15:909.
[211] Kopp S, Wittmann JC, Lotz B. Polymer 1994;35:908.
[212] Kopp S, Wittmann JC, Lotz B. Polymer 1994;35:916.
[213] Sun YJ, Li HH, Huang Y, Chen EQ, Zhao LF, Gan ZH, et al. Macromolecules 2005;38:2739.
[214] Sun YJ, Li HH, Huang Y, Chen EQ, Gan ZH, Yan SK. Polymer 2006;47:2455.
[215] Isayev AI, Chan TW, Shimojo K, Gmerek M. J Appl Polym Sci 1995;55:807.
[216] Alfonso GC, Scardigli P. Macromol Symp 1997;118:323.
[217] Azzurri F, Alfonso GC. Macromolecules 2005;38:1723.
[218] de Gennes PG. Scaling concepts in polymer physics. Ithaca, NY: Cornell University Press; 1979.
[219] Klein J. Nature 1978;271:143.

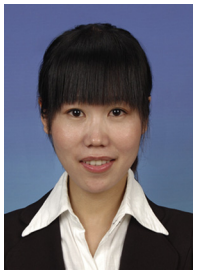

Qi Liu completed her B.S from Qufu Normal University in 2008. She then started an academic project involving postgraduate and doctoral study at the college of Materials Science and Engineering of Beijing University of Chemical Technology under the guidance of Prof. Shouke Yan in the State Key Laboratory of Chemical Resource Engineering. For her postgraduate study, she focused on the orientation induced crystallization of isotactic polypropylene and preparation of microporous membrane from oriented iPP film by stretching.

Xiaoli Sun is currently Associate Professor in the College of Material Sciences and Engineering at Beijing University of Chemical Technology (BUCT). She obtained her Ph.D. in Polymer Physics and chemistry at the Institute of Chemistry, the Chinese Academy of Sciences (ICCAS), in 2009 under the guidance of Prof. Shouke Yan. Thereafter she spent two years as a Postdoctoral fellow at the Kwansei Gakuin University and focused her study in the field of X-ray scattering from soft-matter thin films. In 2011, she became Associate Professor in BUCT. Her current research focuses on the surface and interface effect on the polymer structures and morphologies, crystallization and phase transition behavior of polymer in confined spaces.

Huihui Li is currently an Associate Professor in the College of Material Sciences and Engineering at Beijing University of Chemical Technology (BUCT). She earned her M.S. from Shandong University in 1998 and her Ph.D. in Polymer Science at the Institute of Chemistry, the Chinese Academy of Sciences (ICCAS), in 2004 under the guidance of Prof. S. Yan. After completing her graduate studies, she became an Assistant Professor at the ICCAS. She joined BUCT in 2009. Her current research focuses on the crystallization and multiscale structure manipulation of crystalline/amorphous, crystalline/crystalline polymer blends.

Shouke Yan is Professor in the College of Material Sciences and Engineering at Beijing University of Chemical Technology (BUCT). After receiving a B.S. from Qufu Normal University in 1985, he completed his M.S. in Polymer Science at the Changchun Institute of Applied Chemistry, The Chinese Academy of Sciences (CIAC-CAS). After completing his M.S. study, he joined the CIAC-CAS as an Assistant Professor and then earned his Ph.D. in Polymer Science at the CIAC-CAS under the joint guidance of Prof. Decai Yang and Prof. J. Petermann (Dortmund University, Germany) through a sandwich program between the CAS and the Max-Planck-Society. He then took a position on the research staff at Dortmund University. In 2001, he returned to China through the Hundred Talents Program, to become full Professor at the Institute of Chemistry, The Chinese Academy of Sciences (ICCAS). He has been recognized with several honors, including the Excellent Hundred Talents Award and an NSFC Outstanding Youth Fund. His current research involves surface-induced polymer crystallization, orientation-induced polymer crystallization, phase transition of crystalline polymers and structure-property relationship of polymers.